THE UNIVERSITY OF ALBERTA

MAGNETIC PROPERTIES OF HIGH PRESSURE
$Y_1Ba_2Cu_3O_{7-\delta}$ SUPERCONDUCTOR

BY

JING FU ZHOU

A THESIS

SUBMITTED TO THE FACULTY OF GRADUATE STUDIES AND RESEARCH

IN PARTIAL FULFILLMENT OF THE REQUIREMENTS FOR THE DEGREE

OF MASTER OF SCIENCE

IN

SOLID STATE PHYSICS

DEPARTMENT OF PHYSICS

EDMONTON, ALBERTA

SPRING, 1991

ISBN 0-315-66578-5

THE UNIVERSITY OF ALBERTA

RELEASE FORM

NAME OF AUTHOR JING FU ZHOU

TITLE OF THESIS **MAGNETIC PROPERTIES OF HIGH PRESSURE** $Y_1Ba_2Cu_3O_{7-\delta}$ **SUPERCONDUCTOR**

DEGREE FOR WHICH THESIS WAS PRESENTED **MASTER OF SCIENCE**

YEAR THIS DEGREE GRANTED SPRING 1991

(SIGNED) Zhou Jing Fu

PERMANENT ADDRESS:

P.O. Box 2652

Inst. of Electron.

Academia Sinica

Beijing 100080, P.R.C.

DATED Jan. 30, 1991

THE UNIVERSITY OF ALBERTA

FACULTY OF GRADUATE STUDIES AND RESEARCH

The undersigned certify that they have read, and recommend to the Faculty of Graduate Studies and Research, for acceptance, a thesis entitled **MAGNETIC PROPERTIES OF HIGH PRESSURE $Y_1Ba_2Cu_3O_{7-\delta}$ SUPERCONDUCTOR** submitted by JING FU ZHOU in partial fulfillment of the requirements for the degree of MASTER OF SCIENCE.

J. P. Franck ....

Supervisor

M. Keil ....

J. G. Adler ....

J. A. Tuszynski ....

Date Jan. 30, 1991

Abstract

The USSA-2000 uniaxial split-sphere anvil apparatus has been used to press the $YBa_2Cu_3O_{7-\delta}$ to 10 GPa at 925°C while in hermetically sealed gold capsules. The pressed samples show superconductivity without further oxygen treatment. X-ray measurements show that after pressurization, the lattice parameters a, b, and c do not change. SEM pictures show that after pressurized, the grain size becomes smaller, about 1-5 μm, while the grain size is about 10 μm under the normal pressure. TEM pictures show that there are not fully grown twins between the two fully grown twin boundaries in some regions. All these properties are different from those of normal pressure samples such as higher T_C, lower maximum field for "quasi-de Almeida-Thouless" line ect. SQUID measurements show that the T_C of high pressure sample is about 1-1.4K higher than that of the normal pressure one, and we observed a "quasi-de Almeida-Thouless" line $H \propto [1 - T/92.5]^{3/2}$ up to 2000 Gauss for high pressure sample. We estimate the loop size is in order of 1000 A, which is about the order of twin spacings. We also get the magnetic phase diagram for the high pressure sample. Two theoretical models (superconducting-glass model, oxygen concentration model), their internal relationships, and their interpretation of experimental results have been discussed. A small decrease in T_C of 0.6 K is observed when ^{16}O is substituted by ^{18}O for high pressure sample, and the shift is nonreversible by resubstitution of ^{16}O for ^{18}O at 500°C but is reversible by

resubstitution of ^{16}O for ^{18}O at 900°C. The observation of the oxygen isotope effect of the high pressure samples suggests that the phonon mechanism is important for the electron-pairing in high T_C superconductivity of $Y_1Ba_2Cu_3O_{7-\delta}$. However, owing to the smallness of α, the electron-phonon coupling alone is insufficient to explain such a high T_C in Y-Ba-Cu-O system, so that other mechanisms for the occurrence of superconductivity may also be involved.

ACKNOWLEDGMENTS

Above all I would like to thank Dr. J.P. Franck, my research supervisor, for his guidance, assistance, and interest in this project.

I also wish to thank Dr. Masami Kanzaki and Ms. Dinane Caird of Super Press Lab for their help in doing high pressure experiments. Without their help, it is impossible to carry out the experiments. I would also like to thank Mr. Kejian Wei of Super Press Lab for kindly providing his paper and beneficially discussing about high pressure apparatus, Dr. C.S. Cheng of Physics Department for providing TEM pictures and discussing about the experimental results, and Mr. Baolian Xu of Physics Department for his assistance in plotting many graphics.

Finally, I wish to express my gratitude to the Department of Physics, University of Alberta for financial support in the form of Graduate Assistantship.

TABLE OF CONTENTS

LIST OF FIGURES

Chapter 1

Introduction

Soon after the discovery of Superconductivity around 30K in La-Ba-Cu-O by Bednorz and Muller [3], Chu et al.[4] showed that the Tc of $La_{0.8}Ba_{0.2}CuO_{3-\delta}$ could be increased to above 40K by application of 1.5 GPa hydrostatic pressure. The pressure derivative dTc/dP = 6.1 K/GPa was the largest ever observed in a superconductor. This large influence of pressure led to the idea of replacing La. by a smaller atom, Y in order to produce a "chemical" internal pressure. This resulted in the discovery of $Y_1Ba_2Cu_3O_{7-\delta}$ by Wu et al.[1]. Since then pressure effects on $Y_1Ba_2Cu_3O_{7-\delta}$ have been investigated by several researchers [2,5-9,55] both for hydrostatic pressure and for shock wave pressure [55]. High pressure experiments are very important in discovering new materials and understanding mechanism of new high Tc superconductors.

N. Kawahara et al.[9] carried out high pressure hot-pressing on a cubic-type multianvil high pressure generator. The pressed sample showed semiconducting behavior, the postannealed sample showed a superconducting transition. The reason for the loss of superconductivity after pressed might be the loss of oxygen in the boron nitride capsule during pressing. There could also be chemical reactions inside the capsule.

In our high pressure experiment, we used the USSA-2000 uniaxial split-sphere anvil apparatus to pressurize the $YBa_2Cu_3O_{7-\delta}$ to 10 GPa (100 Kbar). Since Au is very stable, we use gold capsule to prevent any kinds of chemical reaction inside the capsule. The whole assembly (without sample) is fired at 1000°C in Ar for one hour in order to dehydrate all parts completely. This step also prevents any H or O from diffusing in gold capsule during hot pressing. Because of above, we get total different result from that of Kawahara et al. The pressed samples show superconductivity.

The two most fundamental characteristics of superconductivity are the disappearance of resistance and the expulsion of magnetic flux. Therefore along with resistance measurements, magnetic measurements are among the most common in the high T_C literature, beginning with the historic first magnetic confirmation of superconductivity in ceramic LaBaCuO by Bednorz, Takashige, and Muller [10]. Magnetic measurements are particularly convenient for characterizing the new materials because they are non-contact measurements and thus avoid problems in electrically contacting the materials through surface oxide layers or in handling delicate single crystals.

Because of the small size of the samples (2mm in diameter, 1-2mm high), we use SQUID magnetometer to study the their properties.

Two theoretical models (superconducting glass model, oxygen concentration model) have been discussed. Their interpretation of experimental results and their internal relationship have also been discussed.

Finally the observation of oxygen isotope effect for high pressure sample $Y_1Ba_2Cu_3O_{7-\delta}$ is one of the most important achievements of our high pressure experiments. It is discussed in Chapter 2 & 3.

Chapter 2
Experiment

2.1. High Pressure Generation

2.1.1. High Pressure Apparatus

Most of the samples were prepared on the 2000 ton uniaxial split sphere anvil apparatus (USSA-2000) in the Super Press Lab at the University of Alberta [11]. Since this is one of the first studies performed with this high pressure device, a detailed description of the apparatus is included [12,13].

The split sphere anvil apparatus consists of a 2000-ton uniaxial press with a two-stage anvil system capable of achieving pressures above 200 Kbar (20 GPa) at temperature in excess of 2000°C. The first-stage anvil system is a steel sphere split in six parts. The anvils are glued permanently into upper and lower guideblocks and enclose a cubic cavity, 60mm on edge, which contains the second-stage anvil assembly. As shown in Fig 2.1, the second-stage is assembled outside the press and consists of eight tungsten carbide cubes, 32mm on edge, separated by pyrophyllite gaskets, teflon back-up gaskets, and balsa wood spacers. The cubes are truncated at one corner and enclose an octahedral cavity that holds the sample assembly. The sample assembly is an octahedron made of MgO-5%Cr_2O_3. The second stage is

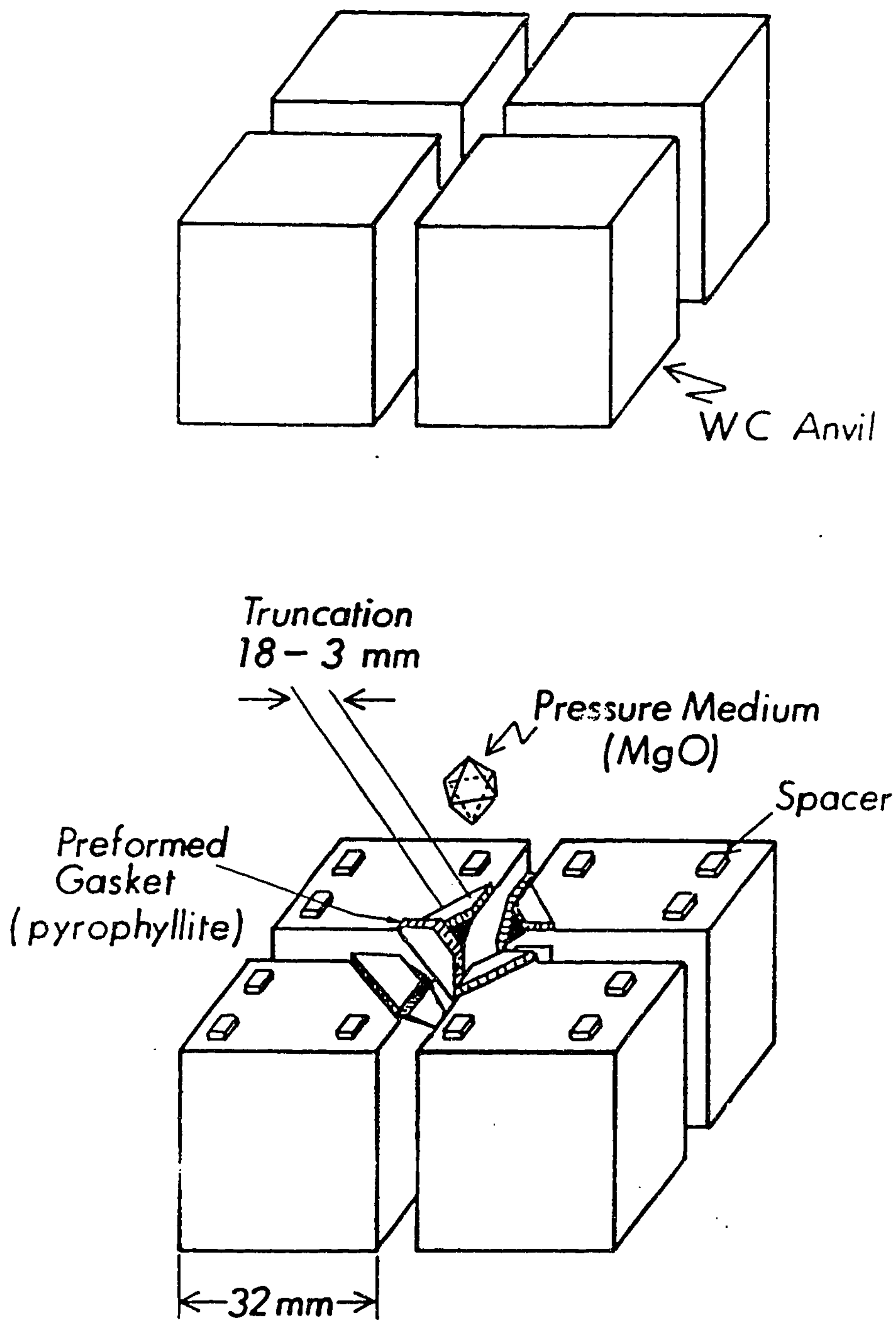

Fig 2.1. The assembly of the second-stage of USSA-2000

electrically insulated from the first stage by phenolic sheets. Electrical insulation between the adjacent cubes is provided by teflon tape.

The sample assembly used in this study is shown in Fig 2.2. The diagram is a cross-section through an MgO octahedron with an edge length of 14.7mm. Heating is provided by the graphite heaters. The Zirconia (ZrO_2) sleeve is a thermal insulator and, together with the Cr_2O_3 of the pressure medium, improves the efficiency of the graphite heaters. The sample is placed in a gold capsule which is electrically insulated from the heater by an MgO sleeve (Platinum capsules were used when the temperature is above 1000°C). The temperature was monitored with a Pt-13%RhPt thermocouple. The contact for the thermocouple wires in the sample assembly is provided by the capsule. The wires cross the heater at the end, and exit the assembly through the edges of a triangular face. The wires are electrically insulated from the heater with alumina and put into a carved out section in one of the triangular faces of the octahedron. The thermocouple wires are taken completely out from the second-stage anvil assembly. The whole assembly (without the sample) installed in the MgO-Cr_2O_3 octahedron is fired at 1000°C in Ar for one hour in order to dehydrate all of the parts completely.

2.1.2. Pressure Calibration

The sample pressure was calibrated against the load

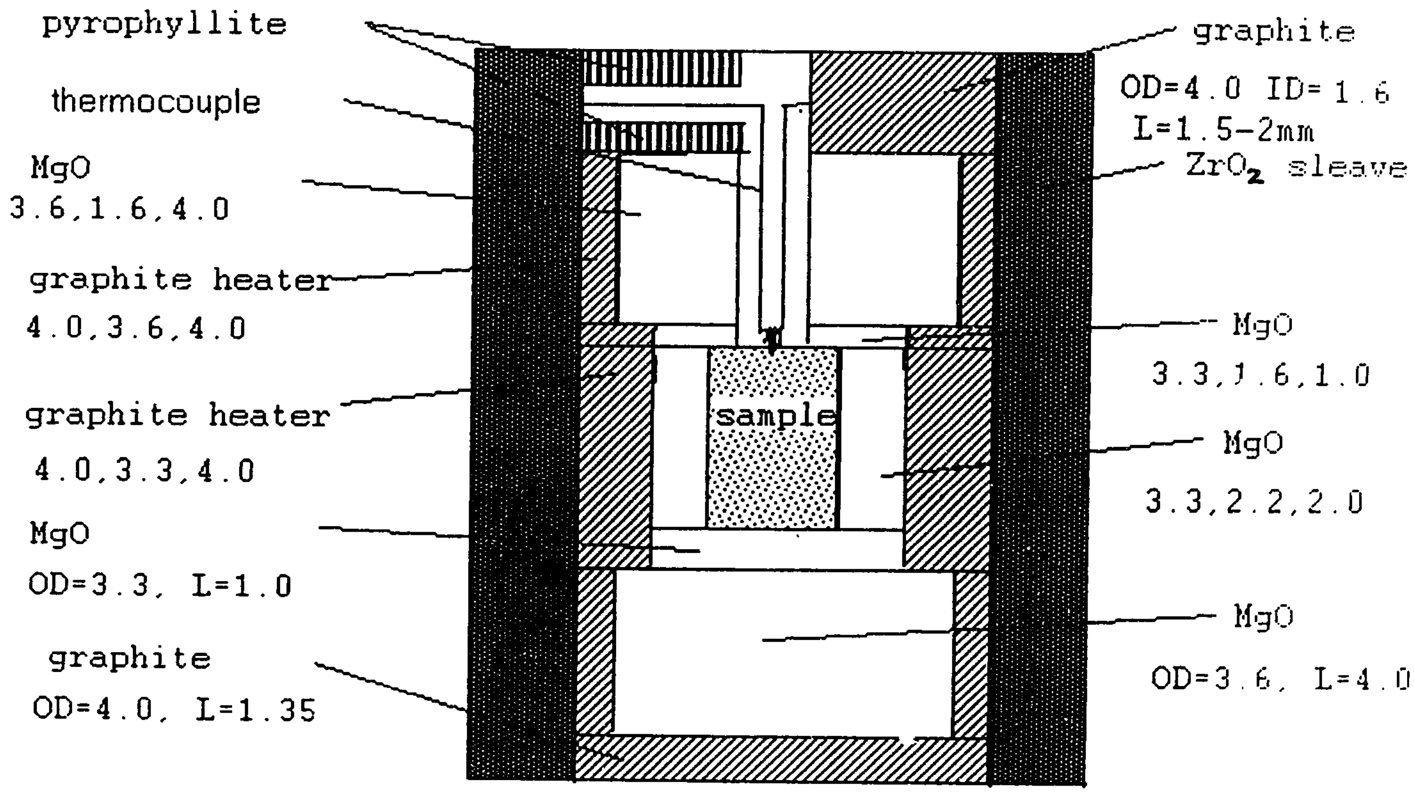

Fig 2.2. The sample assembly for USSA-2000

tonnage by using these transitions: At 1000°C Fe_2SiO_4 $(\alpha-\gamma)$ at 5.3 GPa [14], and Coesite (Cs)- Stishovite (St) at 9.4 GPa [15]. Since most of experiment were carried out around 1000°C, the running pressures were measured based on the pressure calibration at 1000°C. Actually the shift of the calibration curve between 1000°C and 2000°C does not exceed the uncertainty of the calibration. The accuracy and precision of the pressure are estimated to be ±0.2 GPa.

2.1.3. **Temperature Calibration**

Temperatures were measured with Pt-13%RhPt thermocouples and controlled by a programmable controller. The temperature could be controlled to within ±5°C. No correction for the effect of pressure on the thermocouple emf was applied. Our recorded temperature may therefore be somewhat lower than the real temperatures in the hot end of the sample capsules [16,17]. Occasional temperature fluctuations around the set point were typically only a few degrees and too rapid to affect the sample. Independent experiments with the same furnace design and two axial thermal gradient is less than 10°C/2mm near the center of the furnace (Dr. Masami Kanzaki, Univ. of Alberta, personal communication).

2.2. **Sample Preparation**

2.2.1. **Preparation of Normal $Y_1Ba_2Cu_3O_{7-\delta}$ Samples**

A. Sample preparation under normal pressure

The starting mate_ials for the samples were Y_2O_3 (99.99%) , $BaCO_3$ (99.99%) , CuO (99.999%) powders. They were thoroughly mixed, pressed into pellets with 8 Kbar and then calcinated for 24 h in air at 915°C.

The yield was then reground and repressed into pellets with 8 Kbar pressure. This material was sintered in flowing O_2 for 7 h at 925°C then cooled down slowly in O_2 with oven cooling speed to about 35°C before removal from the oven.

The material now is $Y_1Ba_2Cu_3O_{7-\delta}$ Superconductor. It was reground it for high pressure experiment.

B. High pressure process

The superconducting powder was loaded as shown in Section 2.1.1. Different hot-pressings were carried out. Later we have found that different annealing processes did not influence the property of the final products as long as the sample was cooled down slowly to room temperature at a rate of about 3°C/min. Fig 2.3, 2.4, and 2.5 show the processes for samples Mix-Z_3-4 Mix-Z_3-8, Mix-Z_3-6

2.2.2. **Preparation of Isotopically Substituted Samples**

The starting sample [66] was manufactured entirely from high purity ingredients for the substituted sample: CuO^{16} (99.999%), $BaCO_3^{16}$ (99.99%), $Y_2O_3^{16}$ (99.99%). Isotopic substitution was effected by gas-exchange: (1) Calcining in flow oxygen at 915°C for 24 hours, then oven-cooled. (2) After

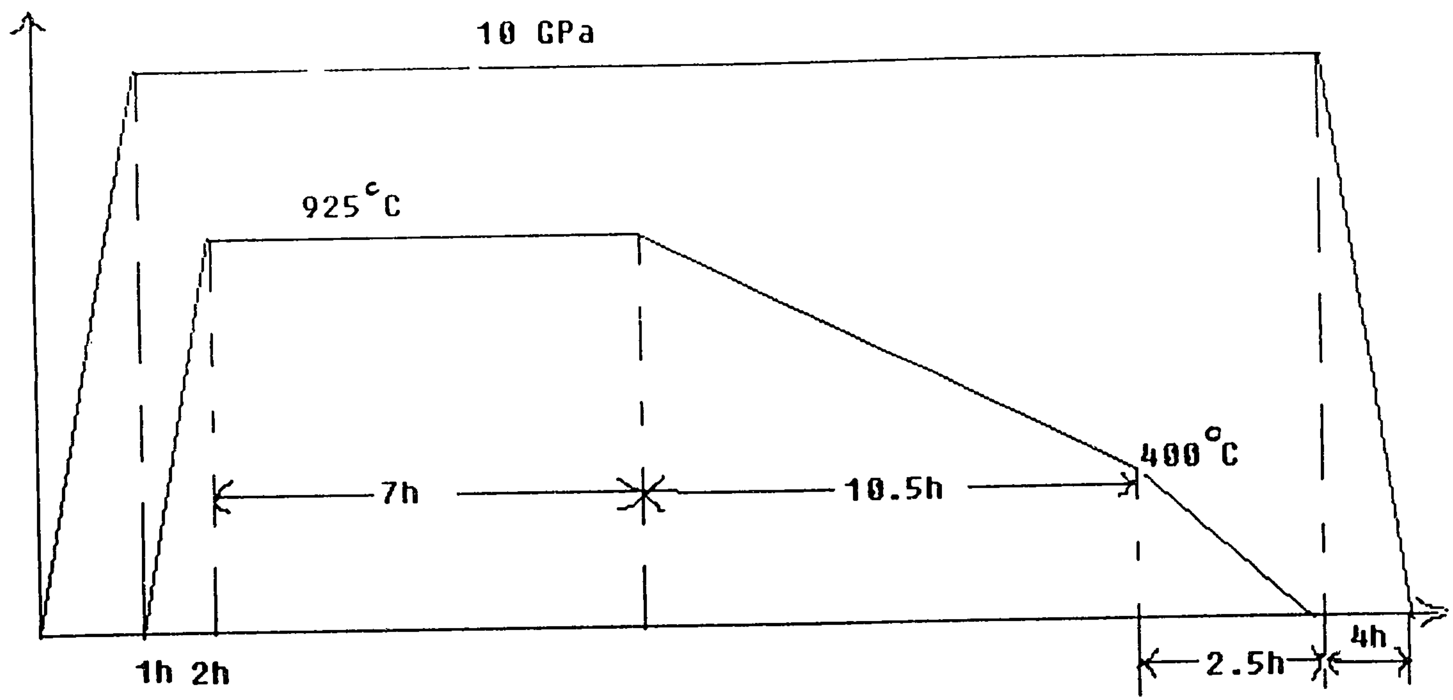

Fig 2.3. High pressure process for Mix-Z_3-4

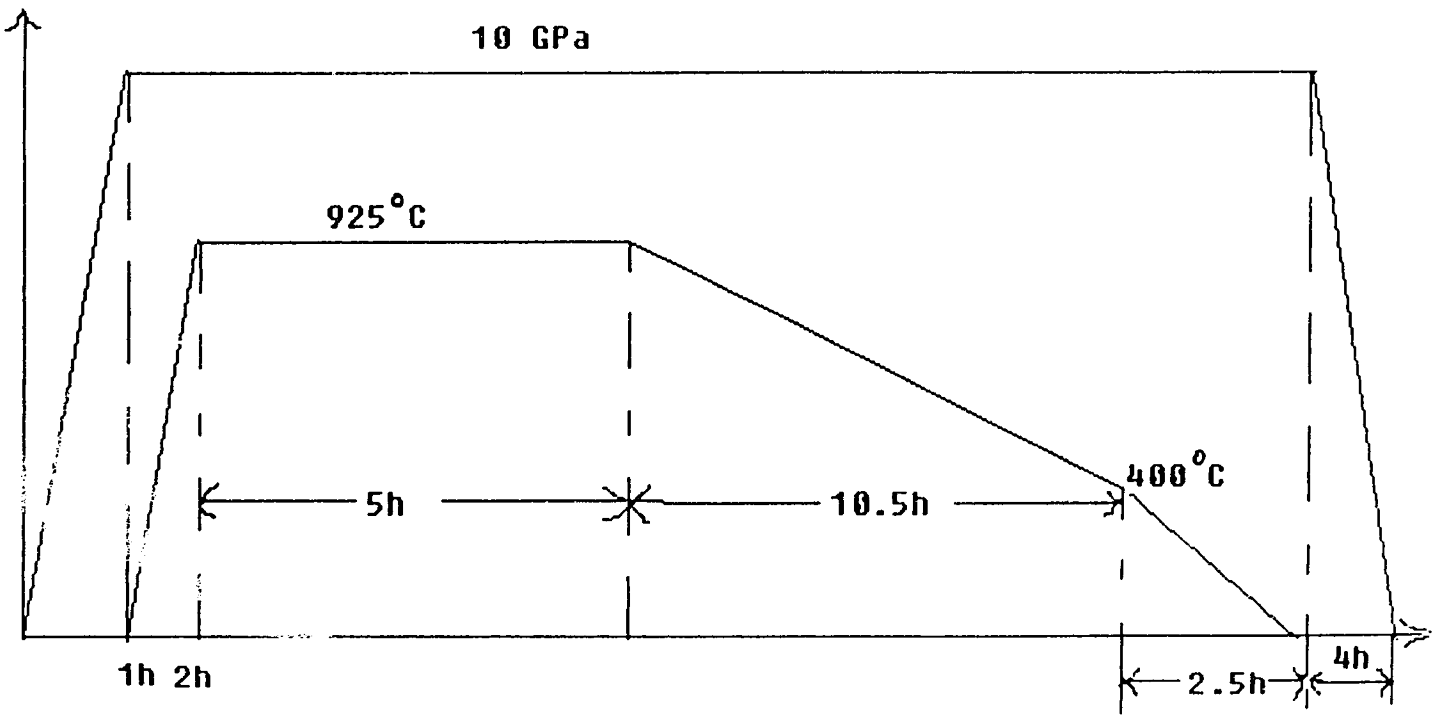

Fig 2.4. High pressure process for Mix-Z_3-8

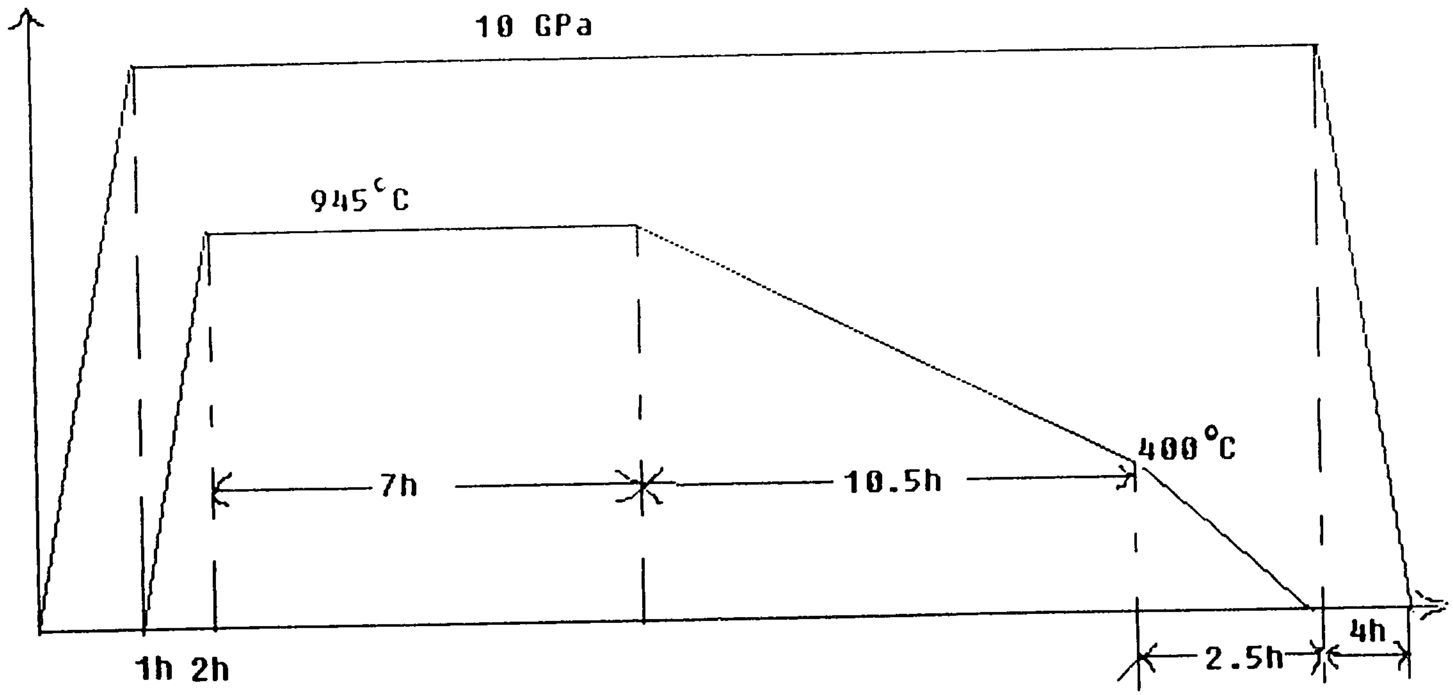

Fig 2.5. High pressure process for Mix-Z_3-6

re-crushing, sintering at 925°C for 7 hours, then oven-cooled. (3) Repeat of step (2). $^{18}O_2$ gas of 99.1 at.-% ^{18}O content was used. The unit cell parameters are a=3.821 A, b=3.885 A, c=3.889 A. SIMS analysis gave a ^{18}O content of 79.7 ± 0.6 at.-% within 10μm of the sample surface, and 85.0 ± 0.2% in the sample core. We applied high pressure to ^{18}O sample as shown Fig 2.6. The result was the 2-IT-1 ^{18}O (HP) sample.

2.3. **Magnetic Measurement**

2.3.1. **The SQUID Magnetometer**

A. Introduction

Quantum interference effects between two Josephson tunnel junctions [18] incorporated in a superconducting ring were first observed by Jaklevic et al.[19] in 1964. These workers showed that the critical current of the double junction was an oscillatory function of the magnetic flux threading the ring, the period being the flux quantum ϕ_0. The implications of this result for instrumentation were quickly realized, and a variety of dc SQUID (Superconducting Quantum Interference Devices) were developed and used. In the late 1960's, the rf SQUID [19-21] appeared. The rf SQUID consists of a single Josephson junction on a superconducting ring, and presumably because only a single junction is required, has become much more widely used than dc SQUID.

B. MPMS System

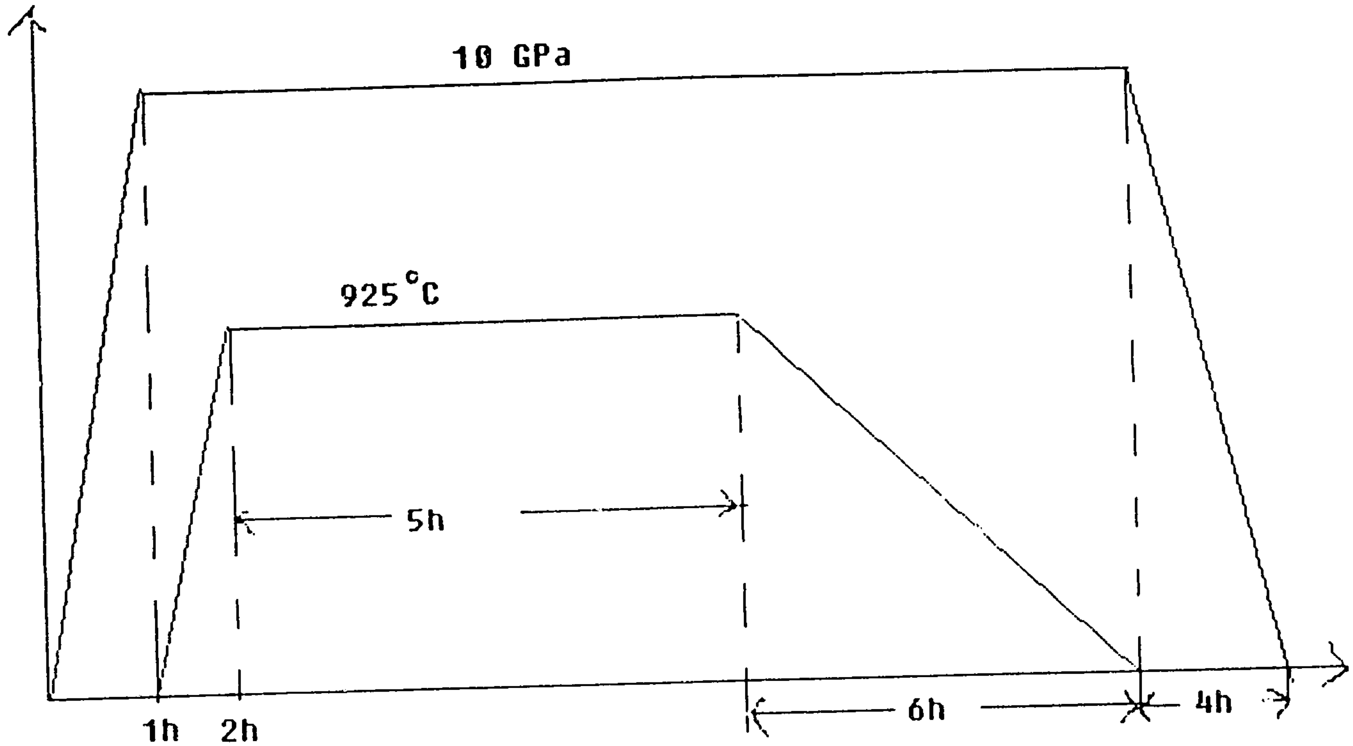

Fig 2.6. High pressure process for 2-IT-1 ^{18}O (HP)

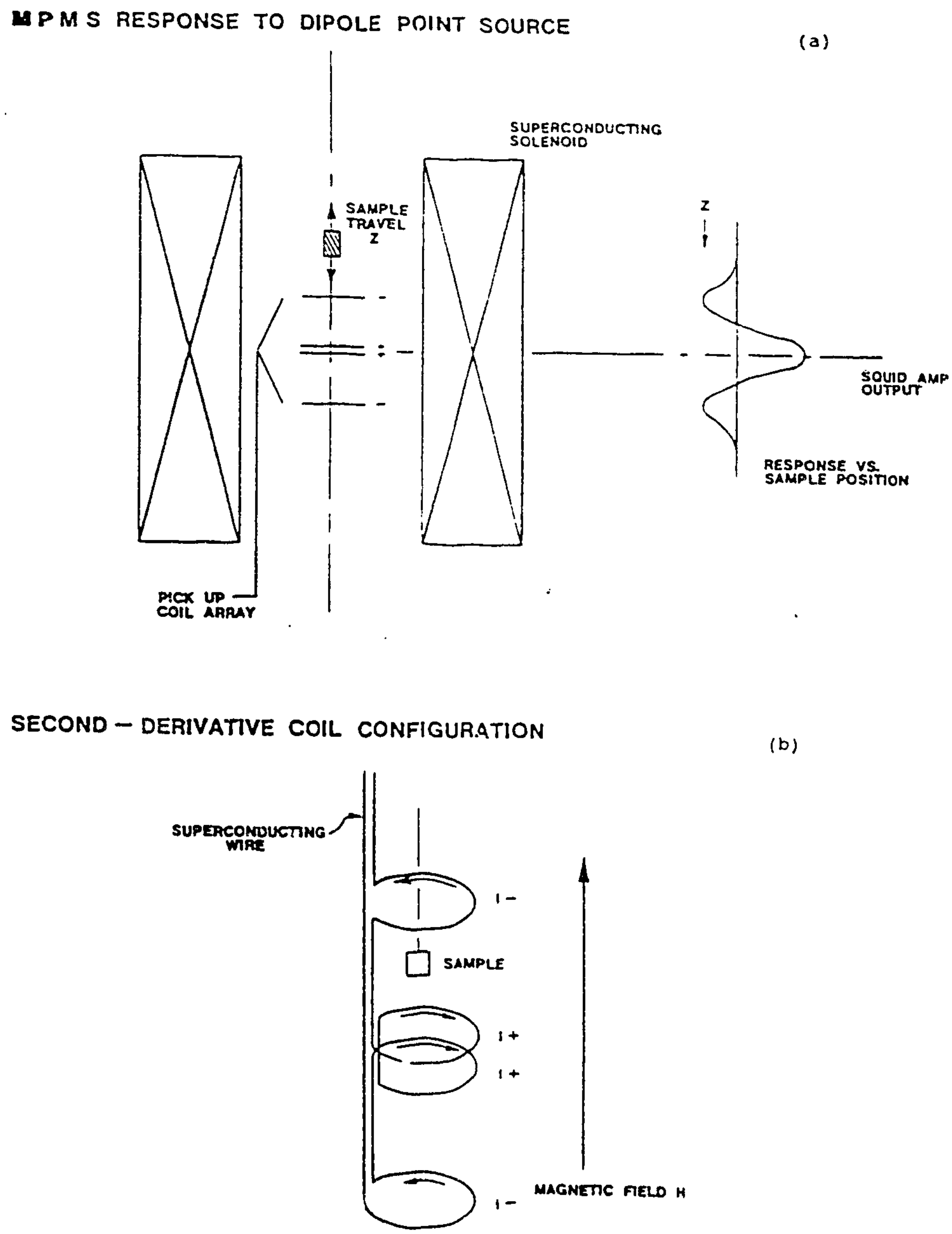

Fig 2.7. (a) MPMS response to dipole point source
(b) Second-derivative Coil Configuration

The Quantum Design Magnetic Property Measurement System or MPMS is a sophisticated analytical instrument configured specifically for the study of the magnetic properties of small experimental samples over a broad range of temperatures and magnetic fields. The system hardware has two major components -- the MPMS dewar and probe assembly, and the associated control system in the MPMS control console. Automatic control and data collection are provided.

The normal measurement technique used in the MPMS system is to position the sample below the detection coils with the sample transport set at its lower limit of travel, then to raise the sample through the coils while measuring the output of the SQUID detector. In its initial position the sample should be far enough below the detection coils so that the SQUID does not detect the sample moment. The sample is then typically measured by repeatedly moving the sample upward some distance and reading the voltage from the SQUID detector. If the SQUID voltage is read out at a large number of points, the voltage can be plotted as a function of the sample position as shown in Fig 2.7(a). One such data set is referred to as a scan.

The SQUID detection loops are configured as a highly balanced second-derivative coil set with a total length of approximately 2.5cm as shown in Fig 2.7(b). This configuration strongly rejects interference from nearby magnetic sources, and allows the system to function without benefit of a superconducting shield arouni the SQUID sensing loops.

The raw data from a measurement are a set of voltage readings taken as a function of position as the sample is moved upward through the sensing loops. At each position, the SQUID output voltage is typically read several times, and many vertical scans can be averaged together to improve the measurement resolution. Both parameters, the number of readings at each point and the number of scans to be averaged, can be set by the user via menu selections.

After the raw data have been collected, the magnetic moment of the sample is computed by numerically summing the square of the individual data points, taking the square root of the result, normalizing the value for the number of data points collected, and multiplying by the system calibration factors. This process minimizes errors due to volume variations in the sample. The magnetic moment calibration for the system is determined by measuring an NBS platinum standard over a range of magnetic fields from +5.5 to -5.5 Telsa, and adjusting the system calibration factors to obtain the correct moment for the NBS standard. The NBS standard is a right circular cylinder approximately 2.5mm in diameter by 2.5mm high. With the pickup coil geometry used in MPMS, samples of this size or smaller are effectively point sources to an accuracy of about 0.1 percent. Since our high pressure sample is about 2mm in diameter by 1-1.5mm high, we have measurement accuracy of about 0.1 percent.

The MPMS technical specifications are in Table 3.1.

Table 3.1 MPMS Technical Specifications

Range of Measurement (emu)
± 2 emu (option to ± 300 emu)
 	
Differential Sensitivity
1×10^{-8} emu in a 2 Telsa magnetic field
 	
Temperature Control at Sample Space
Range: 1.9K to 400K
Stability: <0.05K @ 300K
    <0.01K @ 4.2K
Spatial Variation in Sample Space
    $\pm$0.1K over 8cm
    $\pm$1.0K over 15cm @ 235K
Rate of Temperature Change
    300k to 4.5K in 25 min.
    4.5K to 300K in 25 min.
    Warming 10K/min. @ 390K
    Cooling 15K/min. between 315K and 150K .
 	
Magnet Performance
Field Range: $\pm$5.5 Telsa
Field Stability: 1ppm/hour
Intrinsic Field Uniformity: 0.02% over length of measurement region
Field Resolution: 1 Gauss at 50KGauss, 01 Gauss up to 5 KGauss
Residual Field: After operation at 2 Telsa, 1 Gauss (Typical)
SQUID Control System
Quantum Design Model 2000 VHF SQUID Control Unit.
200 MHz rf System with external feedback. Intrinsic Flux noise less than $1\times10^{-4}\phi_0/\sqrt{Hz}$
	Sample Control
	High resolution .003 mm/step micro-stepper
	Total sample travel available -- 12cm
	Sample slew and acceleration rates computer controlled and user definable
	Transverse rotator available
	Sample tube diameter .355" (9mm)
	
	Computer Controller
	All outputs displayed on 9 inch VDU
	Standard Computer Configuration
	HP Vectra ES, Touch Screen VGA
	Color Monitor, 3.5" and 5.25"
	Floppy, 20M Byte Winchester, 640
	RAM Memory, MS-DOS, HP Think Jet Printer
	
	Dewar System
	Aluminum vapor-shielded dewar
	Fiberglass neck tube with vapor barrier, Helium level meter installed on Temperature Control
	Module
	Helium Capacity 56 liters
	Helium Consumption 6.5 liter/day average
	
	General Requirements
	Ten foot (3.06m) ceiling

	for sample loading 110 VAC, 15 Amps 60Hz Open air flow for pump and electronics cooling Gross weight 650 lbs.(295Kg), floor space required 3' by 7' (1m x 2.2m)

2.3.2. Procedure for Obtaining Magnetic Data

Using MPMS SQUID magnetometer, we first cooled our YBaCuO ceramic sample to low temperature in the small background field of the apparatus. We subsequently applied a field and measured the diamagnetic moment as a function of slowly increasing temperature, obtaining the "zero-field-cooled" (ZFC) curve. We then slowly reduced the temperature back down through the superconducting transition, obtaining the "field-cooled" (FC) curve, this gave a considerably smaller diamagnetic moment. From the graphics, we can determine the transition point, and the irreversibility point where the FC and ZFC curves as a function of temperature merged into a common reversible behavior. Studying these points as a function of the applied field H in the experiments, we can get very useful information.

It is important to recognize the basic difference between the ZFC and FC data. Since flux is initially absent from the sample during zero-field-cooling, the observed diamagnetism after applying a field represents flux exclusion from the sample. This differs fundamentally from the field cooled flux expulsion which characterizes the true Meissner effect.

2.4. **X-ray Powder Diffraction**

X-ray powder diffraction measurements were carried on a Rigaku X-ray Diffractometer System, Model: Geigerflex at the Dept. of Geology, Univ. of Alberta. We use $CoK\alpha$, which $\lambda_{CoK\alpha} = 1.79026 Å$. The operating voltage and current are V = 50KV, I = 20mA. Once we get the diffraction pattern, we can compare it with the known YBaCuO X-ray pattern [22], and we can determine the Miller index (h k l) for each peak and 2θ. Then applying the Bragg Law $2d\sin\theta = n\lambda$ (In our case n=1), we can determine d_{hkl} for each (h k l). From the formula, which is valid for orthorhombic symmetry,

$$\frac{1}{d_{hkl}^2} = \frac{h^2}{a^2} + \frac{k^2}{b^2} + \frac{l^2}{c^2} \qquad 2.1$$

we can calculate a, b, c, for the orthorhombic unit cell.

2.5. **Electron Microscopic Investigation by Scanning Electron Microscope (SEM) and Transmission Electron Microscope (TEM)**

SEM and TEM are powerful techniques to investigate the microstructure of the samples we interested in. From SEM we can get the microstructure information of the sample surface. From TEM we can get the microstructure information inside the sample. Usually TEM has higher resolution than that of SEM but the technique preparing sample for TEM is much more difficult than that of SEM.

SEM measurements were carried on the International Scientific Instrument, Model 60 (ISI-60) at Dept. of Metallurgical Engineering, Univ. of Alberta. The operating voltage is V = 30KV.

TEM measurements were carried on the JEM-100B at Dept. of Physics, Univ. of Alberta. The operating voltage is V = 100KV. The orientation of the sample is placed close to (0 0 1).

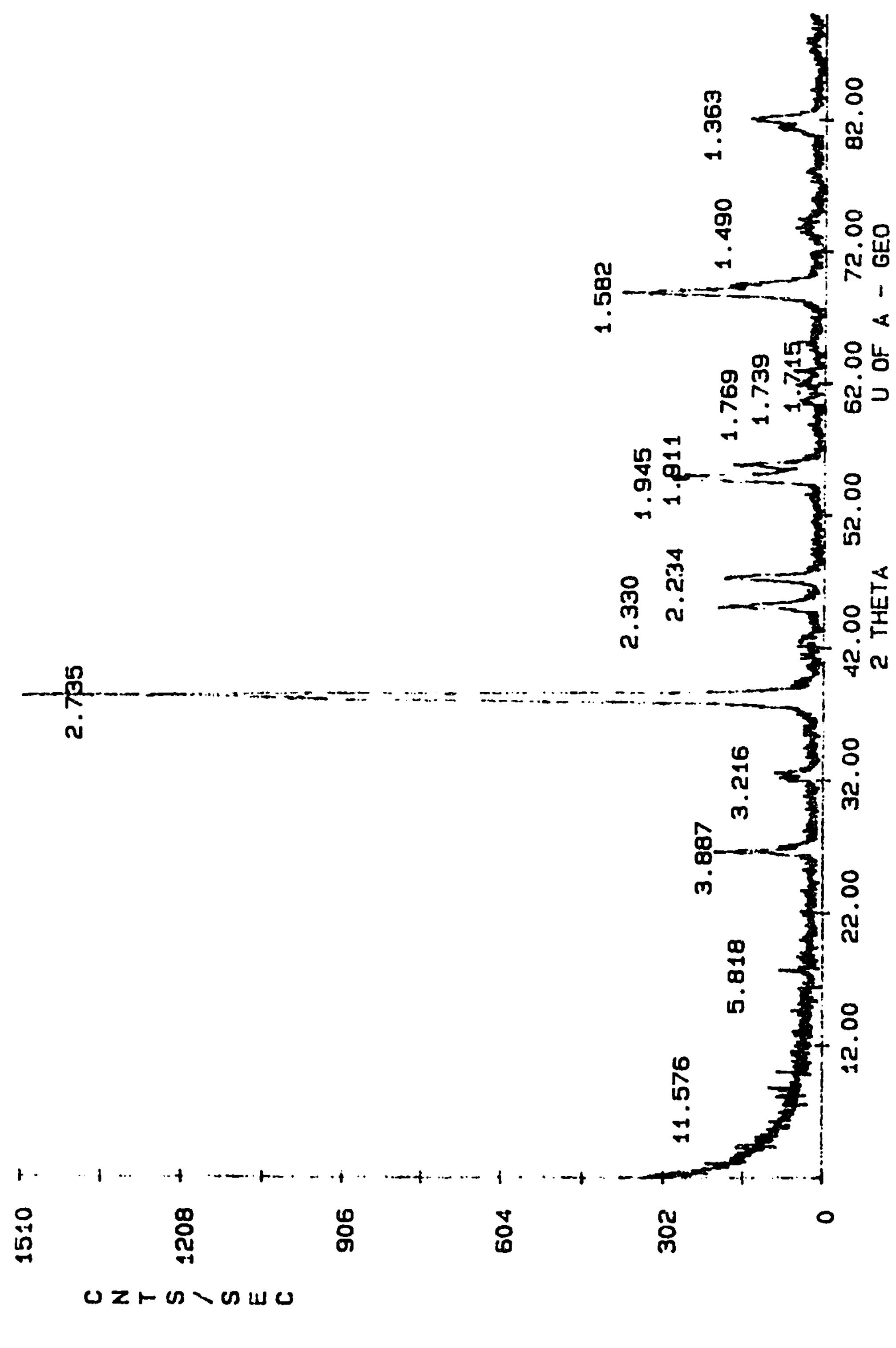
CNTS/SEC
1510
1208
906
604
302
0
11.576
5.818
3.887
3.216
2.735
2.330
2.234
1.945
1.811
1.769
1.739
1.715
1.582
1.490
1.363
12.00
22.00
32.00
42.00
52.00
62.00
72.00
82.00
2 THETA
U OF A - GEO

(a)

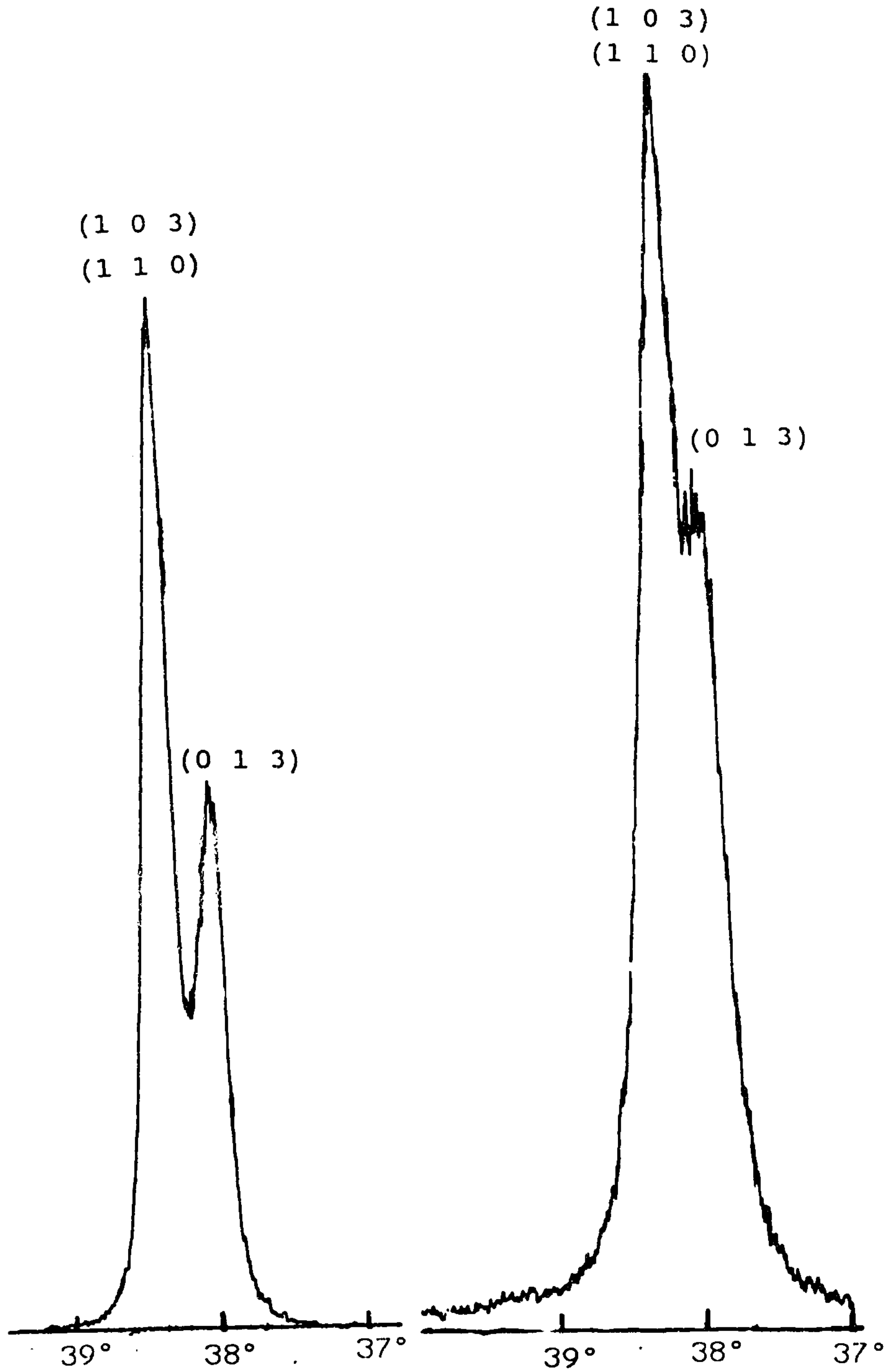

(b)

Fig 3.1. (a) X-ray diffraction pattern for Mix-Z_3-4
(b) X-ray peaks between 37° and 39°
Radiation of $CoK\alpha$

Chapter 3

Results and Analysis

3.1. Introduction

In the following, we will discuss the measurement results and the theoretical models. From the X-ray, SEM, TEM investigations, we can get some of the information about the structure. From the magnetic measurements, we can get T_c and T_{irr} as functions of H, thus we can get the magnetic phase diagram.

Two phenomenological models will be discussed in order to interpret the experimental results. The superconducting-glass model will be used to interpret the difference between FC and ZFC, de Almeida-Thouless line, and the phase diagram. The Oxygen concentration model will be used to interpret the increase of T_c.

Finally, the oxygen isotope effect for the high pressure sample and its meaning for the underlying mechanism for the occurrence of high T_c superconductivity will be discussed.

3.2. Sample Characteristic from X-ray, SEM, and TEM Investigations

A. X-ray Results

The normal pressure and the pressurized powder were characterized by an X-ray diffraction measurement using $CoK\alpha$

radiation. The patterns are the same as shown in Fig 3.1(a) for Tables 3.1, 3.2, and 3.3.

Based on the orthorhombic system [22-24], the lattice parameters are in Table 3.4. From the Table 3.4, we find that lattice parameters of 3 samples are about the same. This suggests that after pressurization, the crystal structure of the sample has not changed. The lattice of this phase is still closely related to the cubic lattice of perovskite. But from Fig 3.1(b) we could see that after pressurization the peaks are broader than those for normal pressure one. This is because after pressurization the grain size become smaller--the size effect.

However, the X-ray data could not provide details of the oxygen-atom positions and occupancies. Clearly, a detailed understanding of the structures of these two forms of $Y_1Ba_2Cu_3O_{7-\delta}$, which requires neutron diffraction techniques.

TABLE 3.1 Powder X-ray diffraction pattern for Mix-Z_3. Orthorhombic unit cell a=3.80(7) A, b=3.88(6) A, c=11.63(6) A, $\lambda_{CoK\alpha}$ = 1.79026 A, P=1 bar

h k l	2θ(°)	d (A)	I/I_0 (%)
0 0 2	17.7	5.818	3
0 0 3	26.8	3.870	10
1 0 0	27.2	3.800	4
1 0 2	32.6	3.189	5
0 1 3	38.1	2.746	48
1 0 3 1 1 0	38.4	2.723	100
1 1 2	42.6	2.464	3
0 0 5	45.2	2.329	12
1 1 3	47.4	2.227	14
0 2 0 0 0 6	54.9	1.940	21
2 0 0	56.0	1.907	12
1 1 5	60.7	1.772	3
0 1 6 0 2 3	62.1	1.735	2
2 0 3 2 1 0	63.0	1.713	2
1 2 2 1 2 3	69.0	1.580	28
2 1 3	69.6	1.567	13

TABLE 3.2 Powder X-ray diffraction pattern for Mix-Z_3-4 sample. Orthorhombic unit cell a=3.82(0) A, b=3.88(5) A, c=11.63(7) A, $\lambda_{CoK\alpha}$=1.79026A, P=100Kbar

h k l	2θ(°)	d (A)	I/I_0 (%)
0 0 2	17.7	5.818	3
0 0 3	26.7	3.877	10
1 0 2	32.6	3.189	5
0 1 3	38.0	2.749	48
1 0 3 1 1 0	38.3	2.729	100
1 1 2	42.6	2.464	3
0 0 5	45.2	2.329	12
1 1 3	47.4	2.229	14
0 2 0 0 0 6	54.9	1.940	21
2 0 0	55.9	1.910	12
1 1 5	60.7	1.772	3
0 1 6 0 2 3	62.2	1.733	2
1 2 2 1 2 3	69.0	1.580	28

TABLE 3.3 Powder X-ray diffraction pattern for Mix-Z_3-6 sample. Orthorhombic unit cell a=3.82(0) A, b=3.89(2) A, c=11.63(9) A, $\lambda_{CoK\alpha}$=1.79026A, P=100Kbar

h k l	2θ(°)	d (A)	I/I_0 (%)
0 0 2	17.7	5.818	3
0 0 3	26.7	3.870	10
1 0 2	32.5	3.204	5
0 1 3	38.0	2.749	48
1 0 3 1 1 0	38.3	2.729	100
1 1 2	42.5	2.470	3
0 0 5	45.1	2.334	12
1 1 3	47.3	2.231	14
0 2 0 0 0 6	54.9	1.943	21
2 0 0	55.9	1.910	12
1 1 5	60.7	1.772	3
0 1 6 0 2 3	62.0	1.738	2
1 2 2 1 2 3	68.8	1.584	28

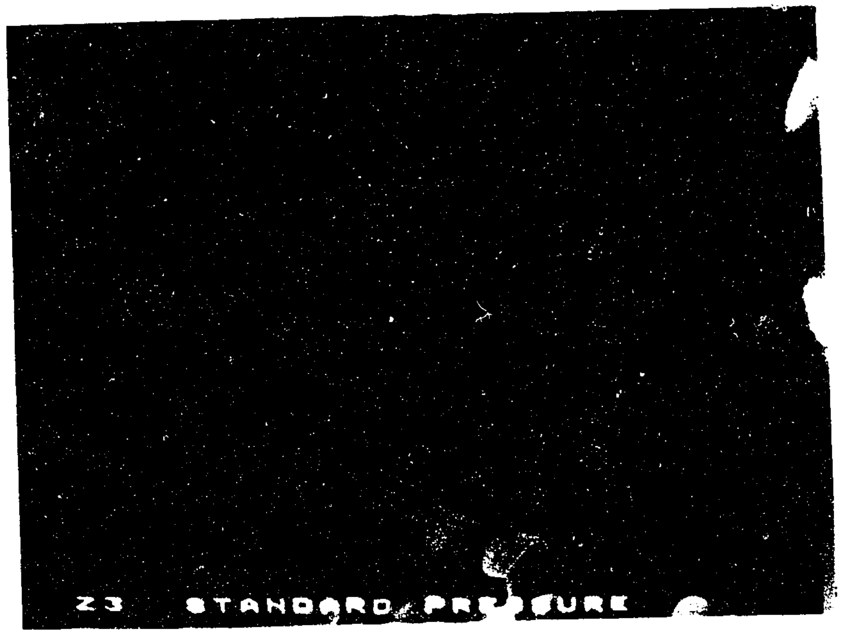

(a)

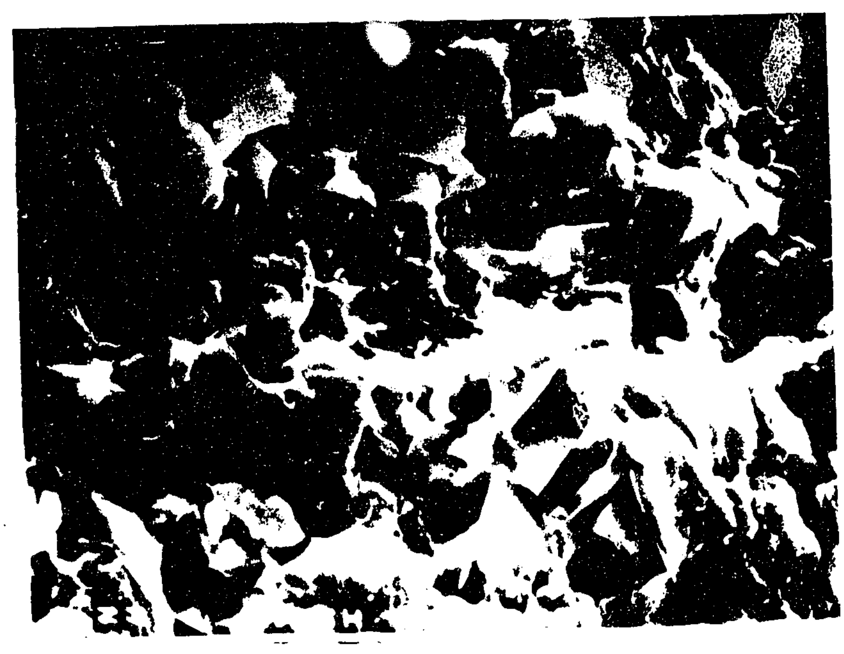

(b)

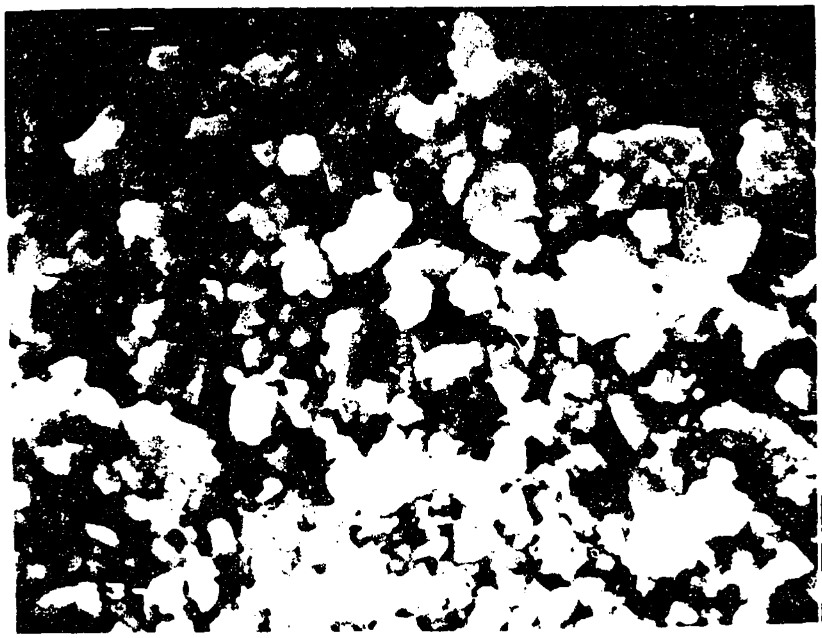

(c)

Fig 3.2. (a) SEM picture for standard pressure sample
(b) & (c) SEM pictures for pressurization samples
[(a) for Mix-Z_3, (b) for Mix-Z_3-4 (c) for Mix-Z_3-8]

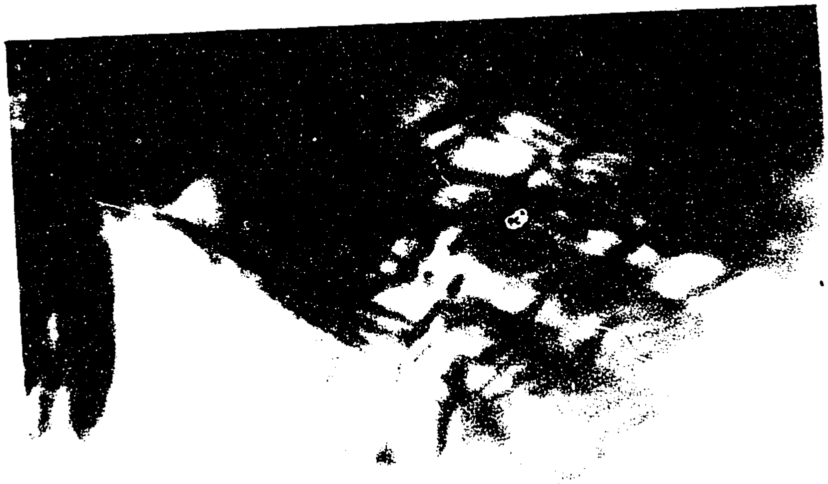

Fig 3.3. TEM picture for selected area (After C.S. Cheng)

TABLE 3.4 Lattice Parameters

Sample	a (A)	b (A)	c (A)
Mix-Z_3 (NP)	3.80(7)	3.88(6)	11.63(3)
Mix-Z_3-4(HP)	3.82(0)	3.88(5)	11.63(7)
Mix-Z_3-6(HP)	3.82(0)	3.89(2)	11.63(9)

B. **SEM Results**

Samples Mix-Z_3, Mix-Z_3-4 Mix-Z_3-6 were observed by scanning electron microscope (SEM). From SEM analysis, for the standard pressure, the grain size is about 10 μm (Fig 3.2a); after pressurization, the grain size becomes smaller, which is about 1--5 μm (Fig 3.2b,c). From Fig 3.2, we could see the pressurized samples are denser than the standard pressure samples. The difference between sample Mix-Z_3-4 and Mix-Z_3-6 might occur because of the higher sintering temperature for sample Mix-Z_3-6. For Mix-Z_3-4 sample, the highest sintering temperature is 925°C, but for Mix-Z_3-6 is 945°C. It seems that higher sintering temperature produces smaller grains of samples. The change of microstructure in high pressure samples might cause the change of physical properties of superconducting materials.

C. TEM Results

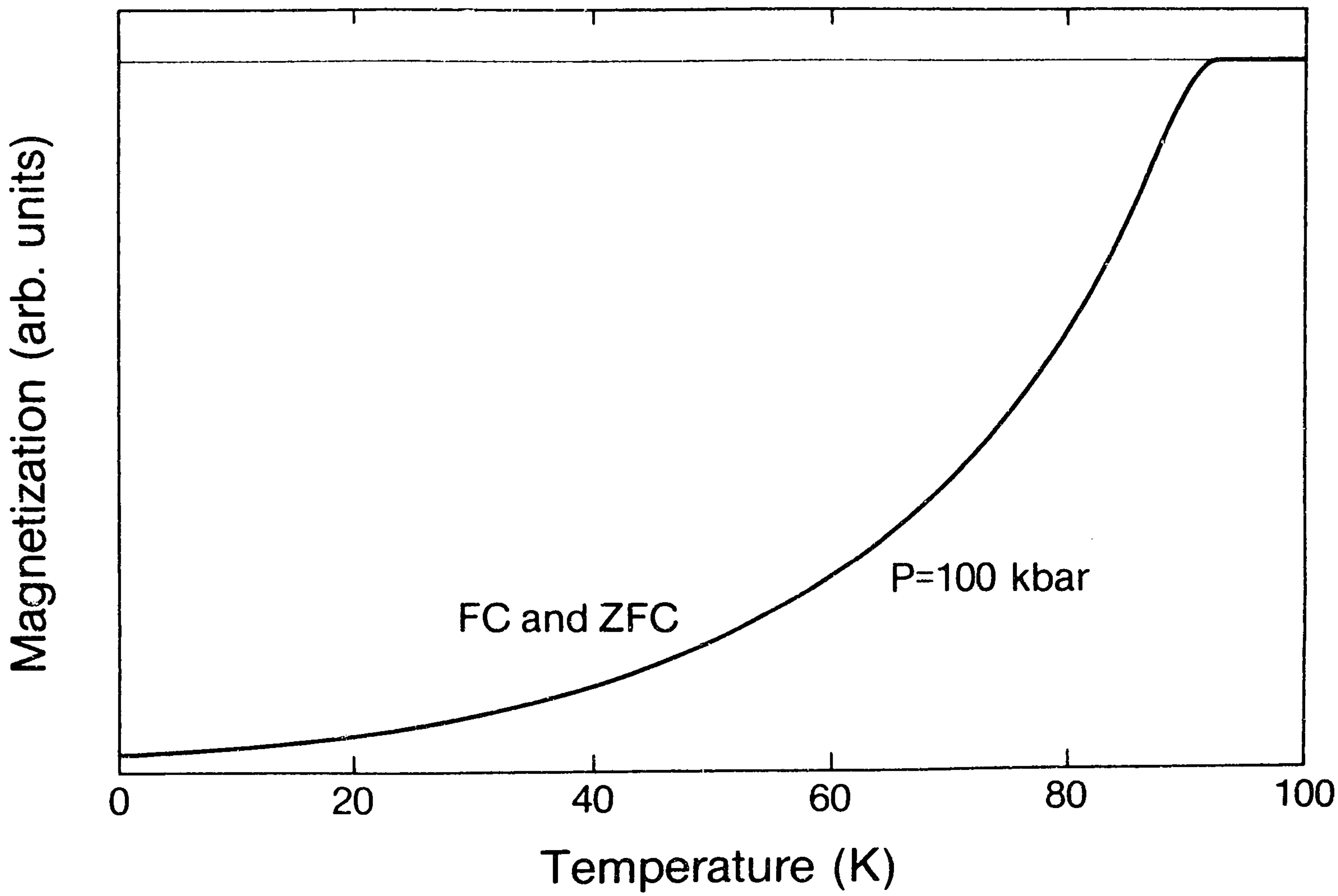

Fig 3.4. FC and ZFC at H=0.1 Oe for pressurization sample (After S. Gygax et al.)

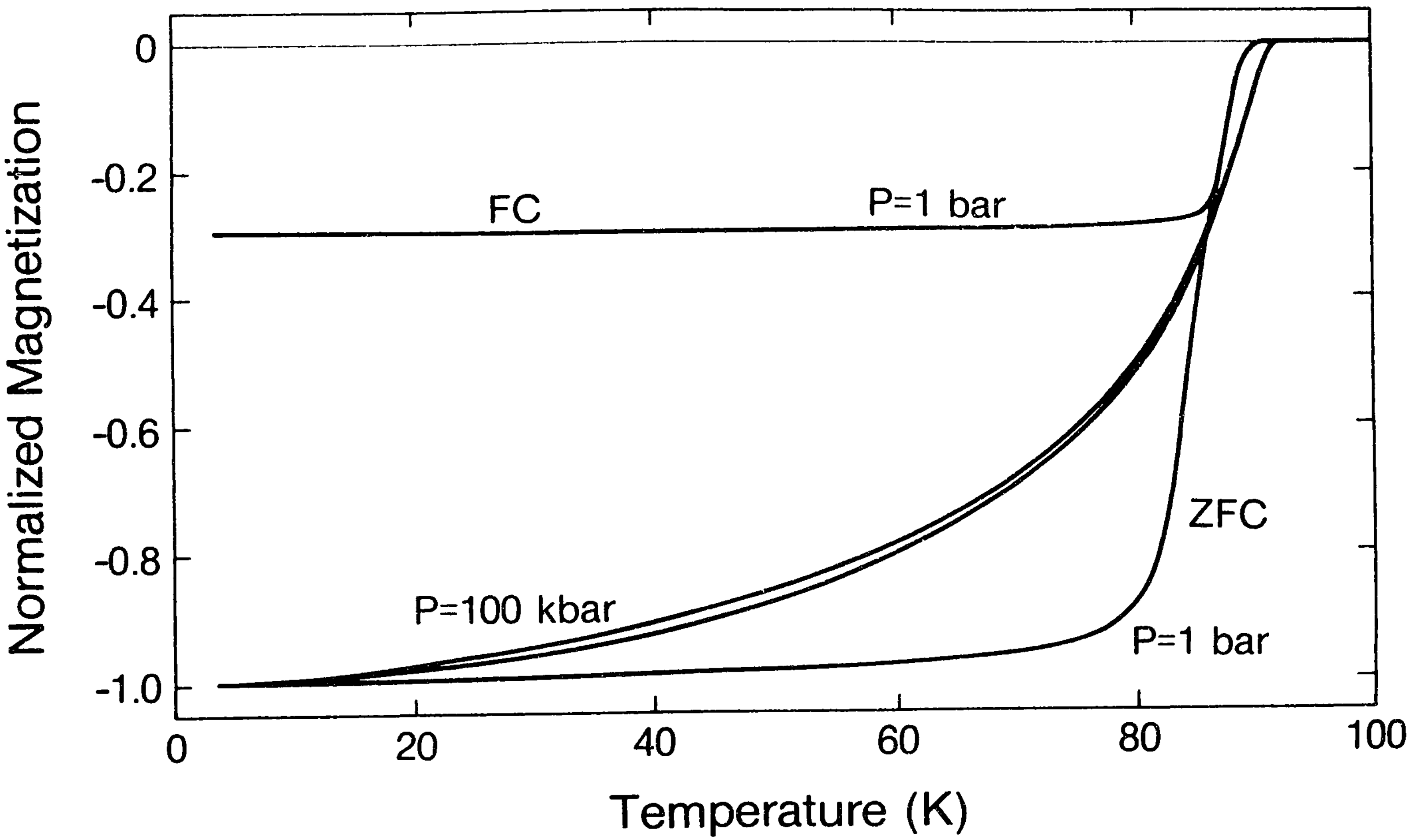

Fig 3.5. FC and ZFC at H=0.5 Oe for pressurization sample
(After S. Gygax)

Fig 3.3 is taken by Dr. C.S. Cheng. The microstructure of the pressurized samples is different from that of the normal ones. In some regions, between two fully grown twins there are not fully grown twins, and there is microcracking on the twin boundaries. These properties are different from those of normal pressure pressure one. In normal ones, you could see that twins are fully grown, their boundaries are clear, and there is no microcracking on the boundaries.

3.3. **Magnetic Measurement**

3.3.1. **Sample Mix-Z3-6 Measurement Results**

Low field (up to 1 Gauss) magnetization M vs T (temperature) measurement was carried out by Prof. Suso Gygax et al. in Dept. of Phys., Simon Fraser Univ., Burnaby, British Columbia, on the pressurized samples.

Fig 3.4 & 3.5 show his measurement results. Fig 3.4 shows at H=0.1 Oe the field-cooled (FC) curve and the zero-field-cooled (ZFC) curve are the same. This means that at H=0.1 Oe, we have perfect Meissner effect. This seems to be a sample which has negligible pining. He made ac-loss measurement. The ac-loss peak seem to be absent (at least within the sensitivity they were customarily using). The flux lattice must be quite rigid to account for the absence of loss without pinning. Fig 3.5 shows at H=0.5 Oe, for normal pressure sample, T_c = 91.5 K; for high pressure

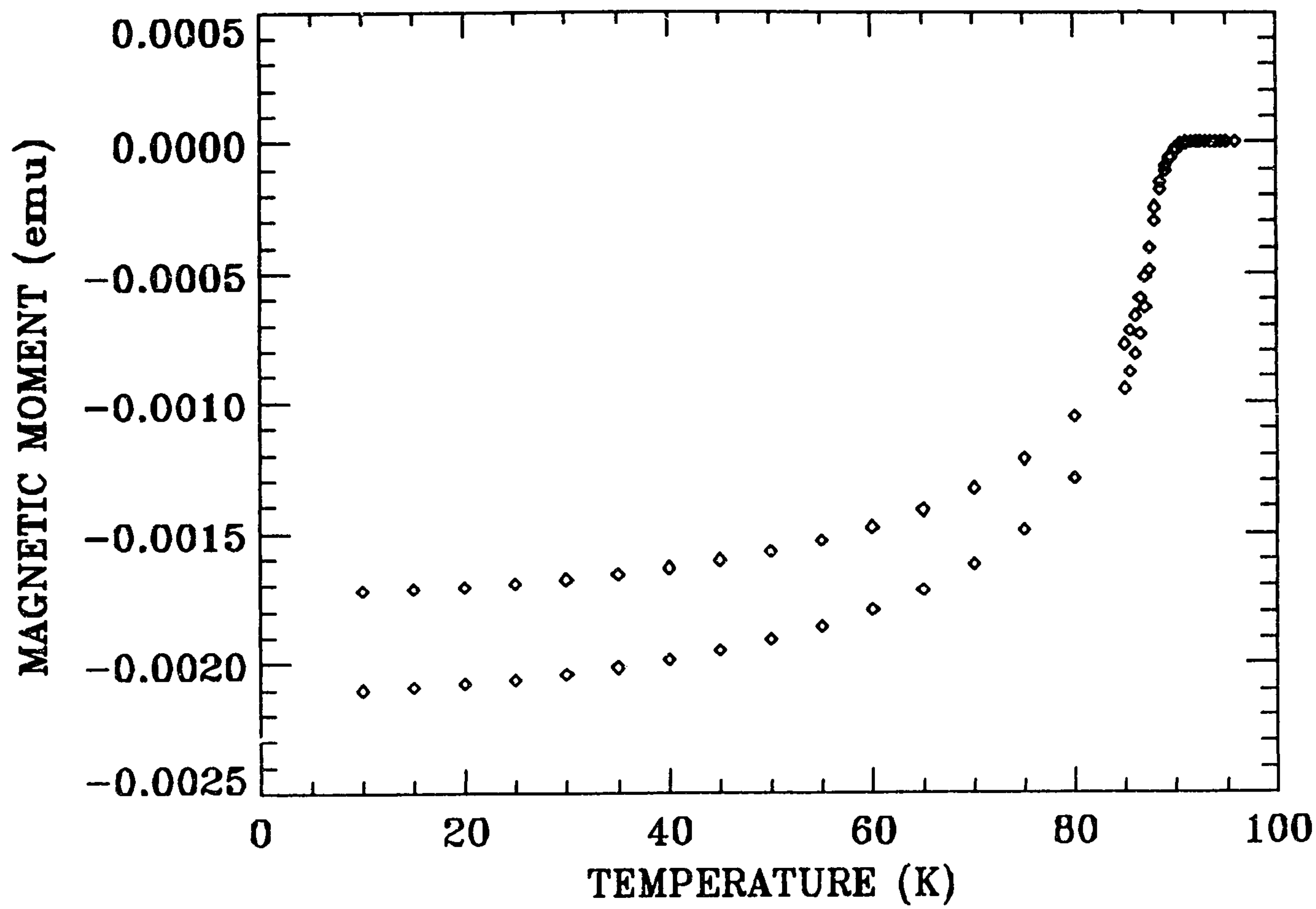

Fig 3.6. M vs T at H = 10 Gauss for Mix-Z_3 Powder

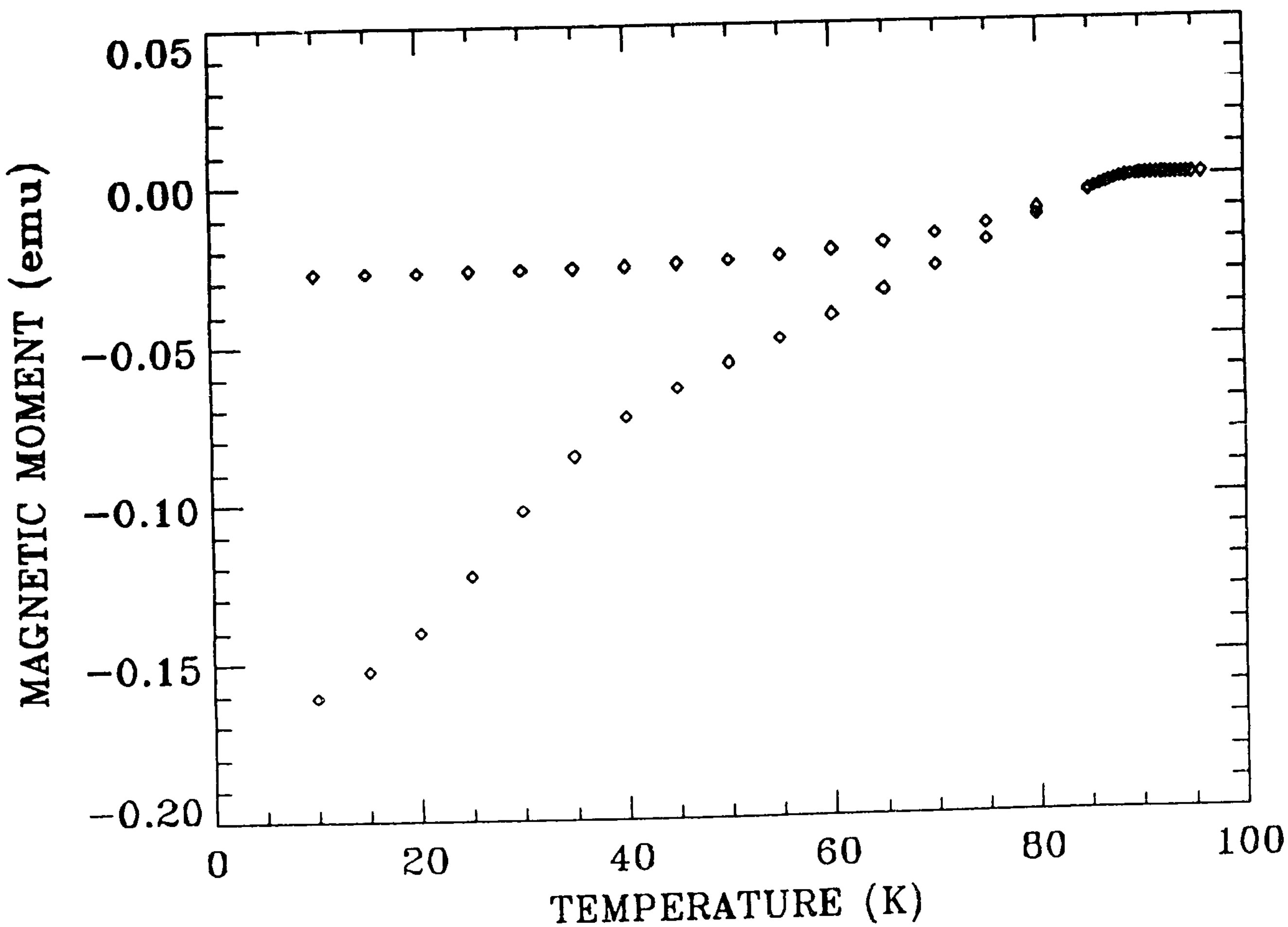

Fig 3.7. M vs T at H = 1K Gauss for Mix-Z_3 Powder

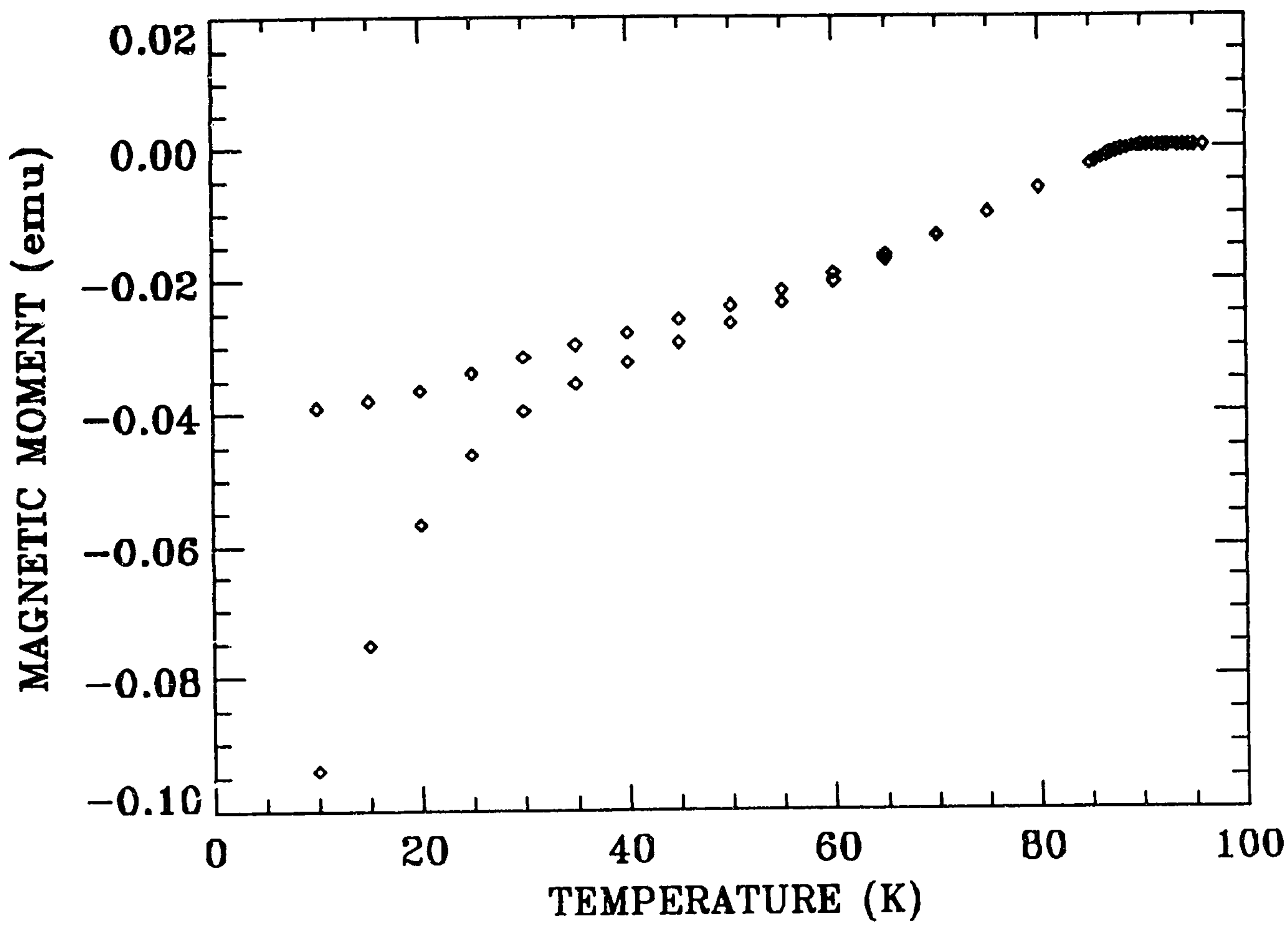

Fig 3.8. M vs T at H = 10K Gauss for Mix-Z_3 Powder

sample, T_c = 92.5 K. ZFC and FC curves are separating. The transition temperature of high pressure sample is obviously higher than that of normal pressure sample.

3.3.2. **Sample Mix-Z3-Powder Measurement Results**

Fig 3.6-3.8 are three of measurement results for the powder of normal pressure sample. From those measurement graphics, I can pick up the transition temperature T_c, the critical temperature T_{irr} of irreversible curves with the same method stated in Section 2.3.2.

TABLE 3.5 T_c, T_{irr}, of Mix-Z_3-Powder Sample

H (Gauss)	log H (log G)	T_{irr} (K)	T_c (K)
2	0.30103	90.0	91.25
10	1.00000	91.0	91.15
25	1.39794	90.5	91.20
50	1.69897	90.5	91.00
100	2.00000	90.0	91.25
250	2.39794	90.5	91.10
500	2.69897	89.0	91.10
1000	3.00000	87.0	91.08
2000	3.30103	86.0	91.04
5000	3.69897	83.5	91.10
10000	4.00000	80.0	90.78
20000	4.30103	75.0	90.80
30000	4.47712	75.0	90.80
50000	4.69897	70.0	90.70

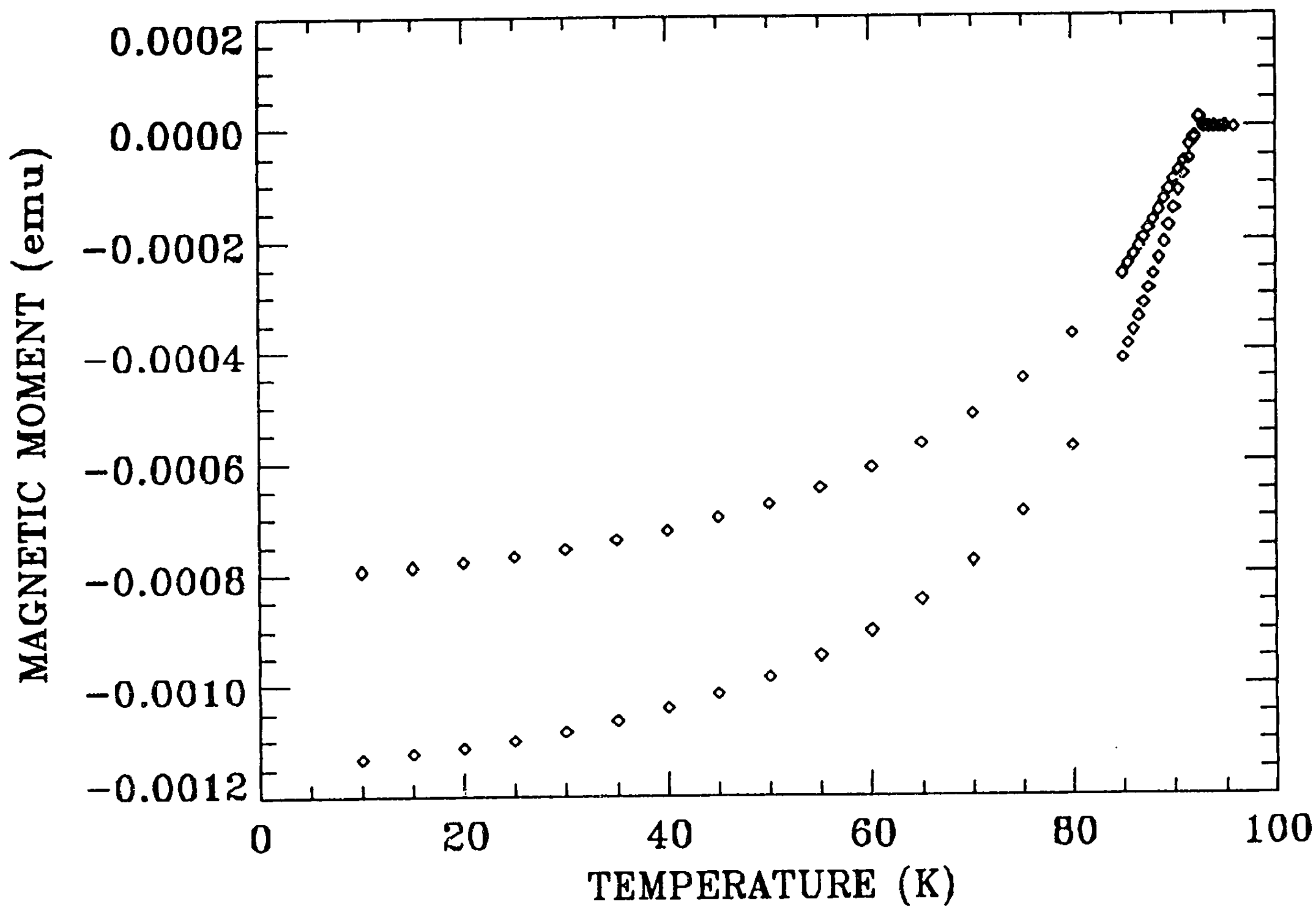

Fig 3.9. M vs T at H = 10 Gauss for Mix-Z_3-8

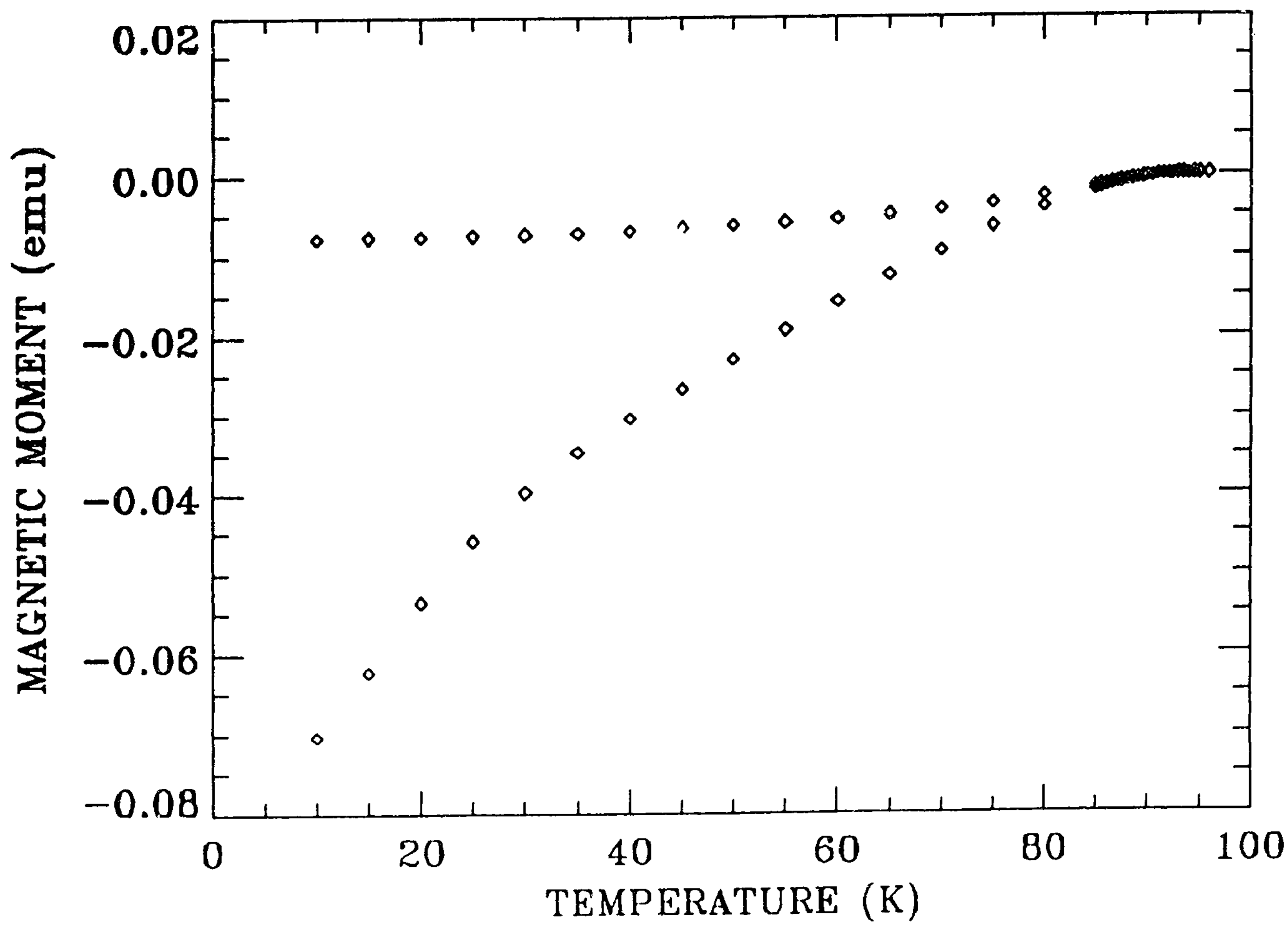

Fig 3.10. M vs T at H = 1K Gauss for Mix-Z_3-8

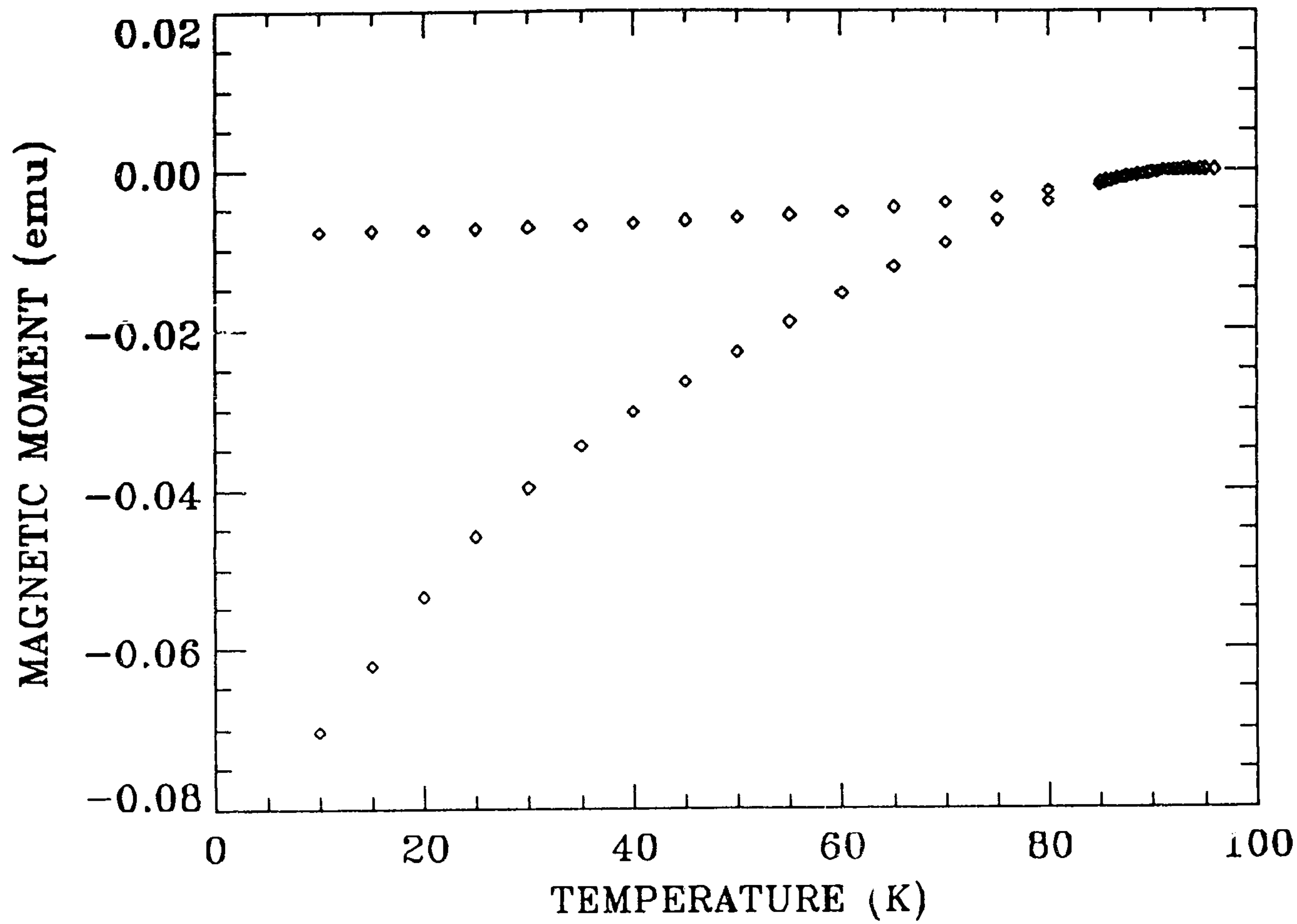

Fig 3.11. M vs T at H =10K Gauss for Mix-Z_3-8

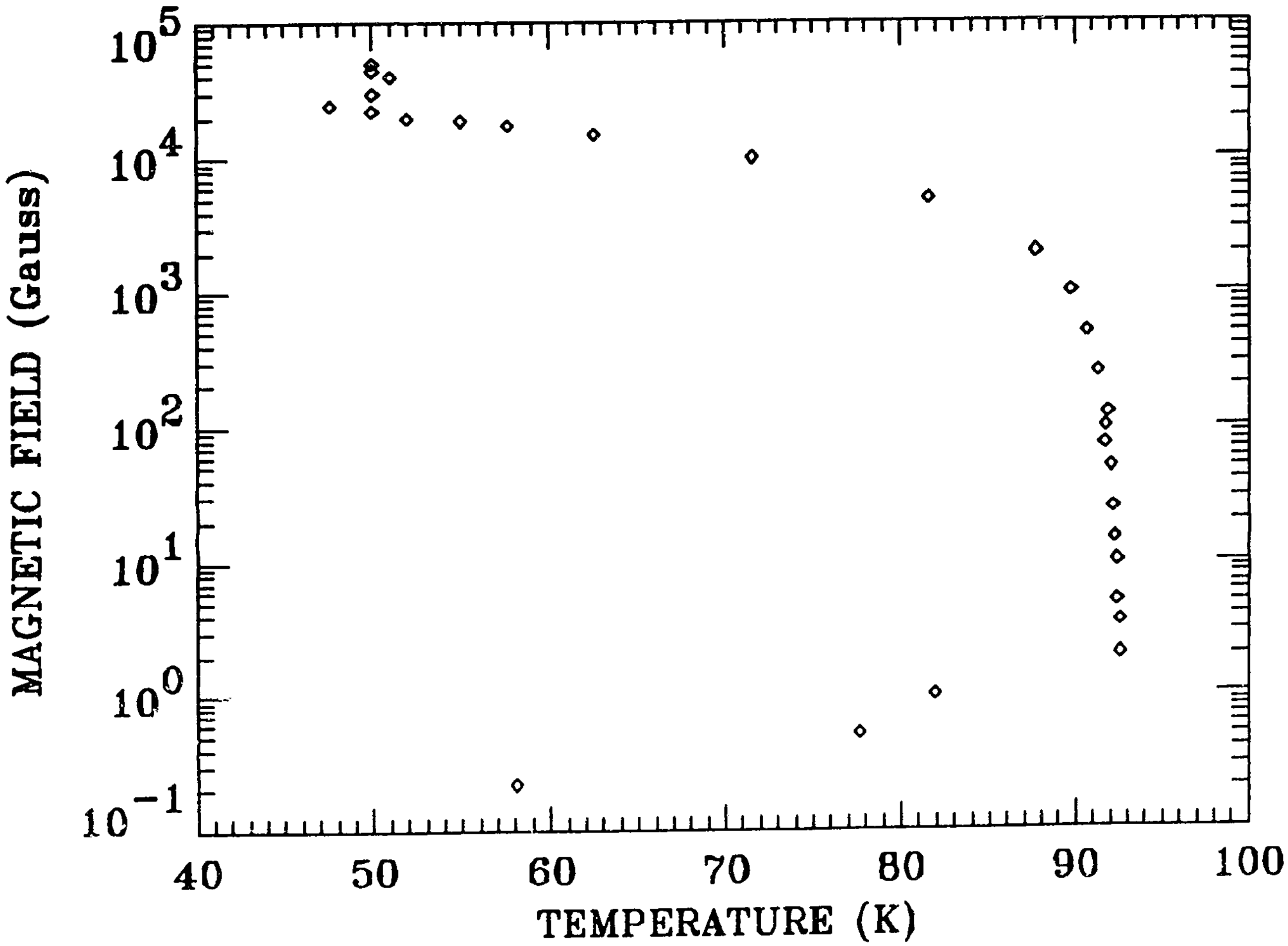

Fig 3.12. M vs T_{irr} for Mix-Z_3-8 (The measurements were taken by Prof. S. Gygax et al. for $H \leq 1$ Gauss)

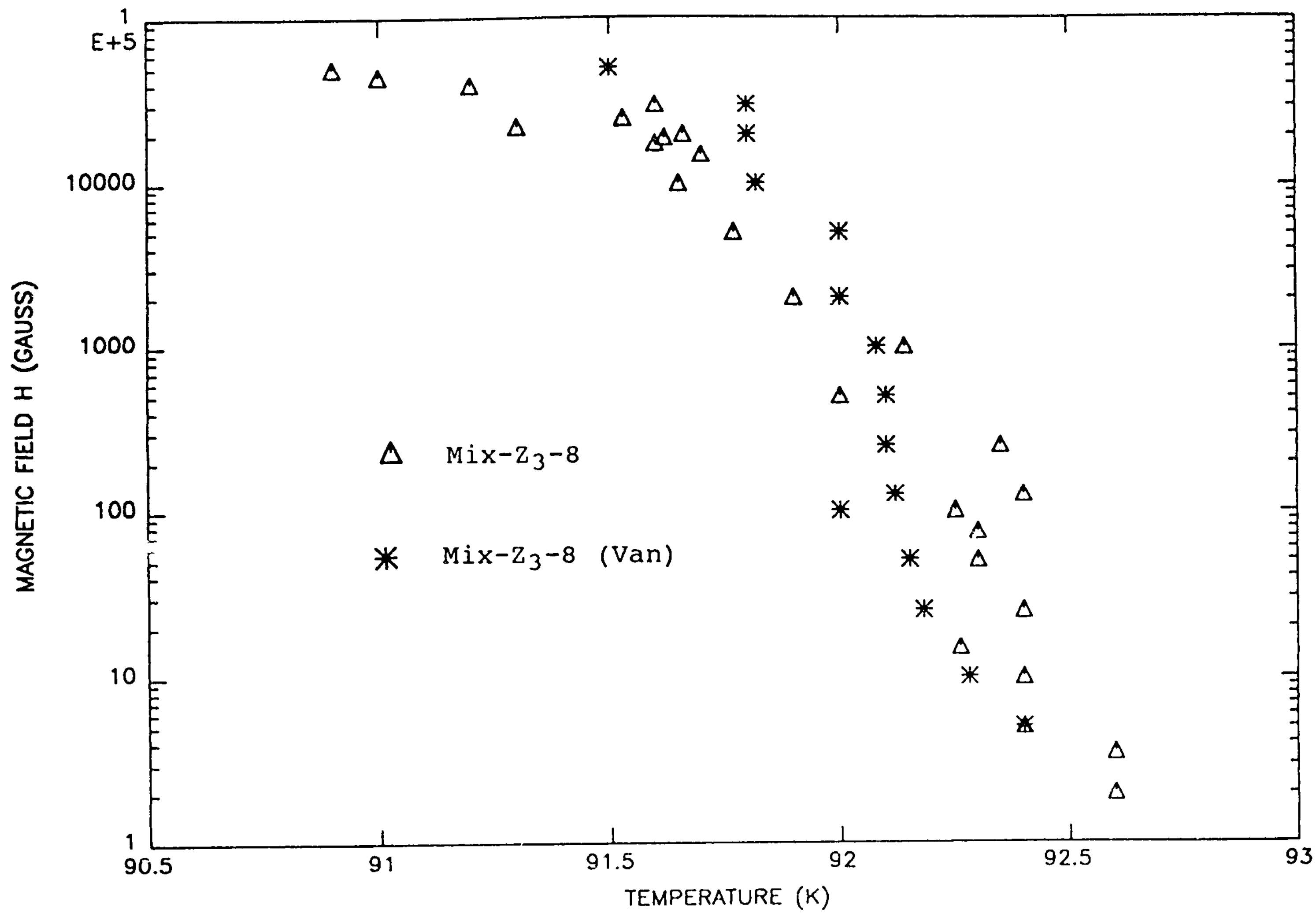

Fig 3.13. Comparison of T_c for Mix-Z_3-8 (Van) & Mix-Z_3-8

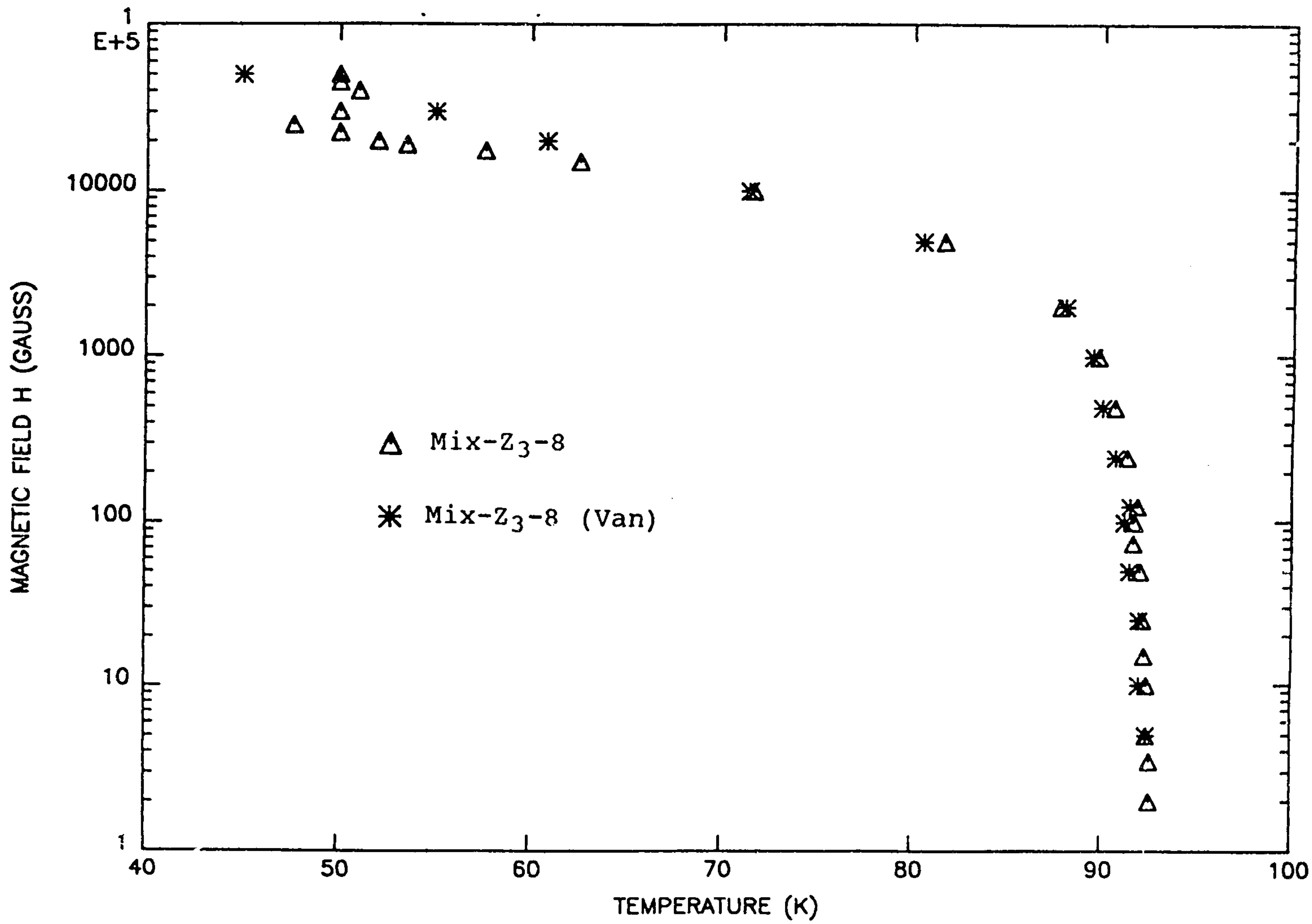

Fig 3.14. Comparison of T_{irr} for Mix-Z_3-8 (Van) & Mix-Z_3-8

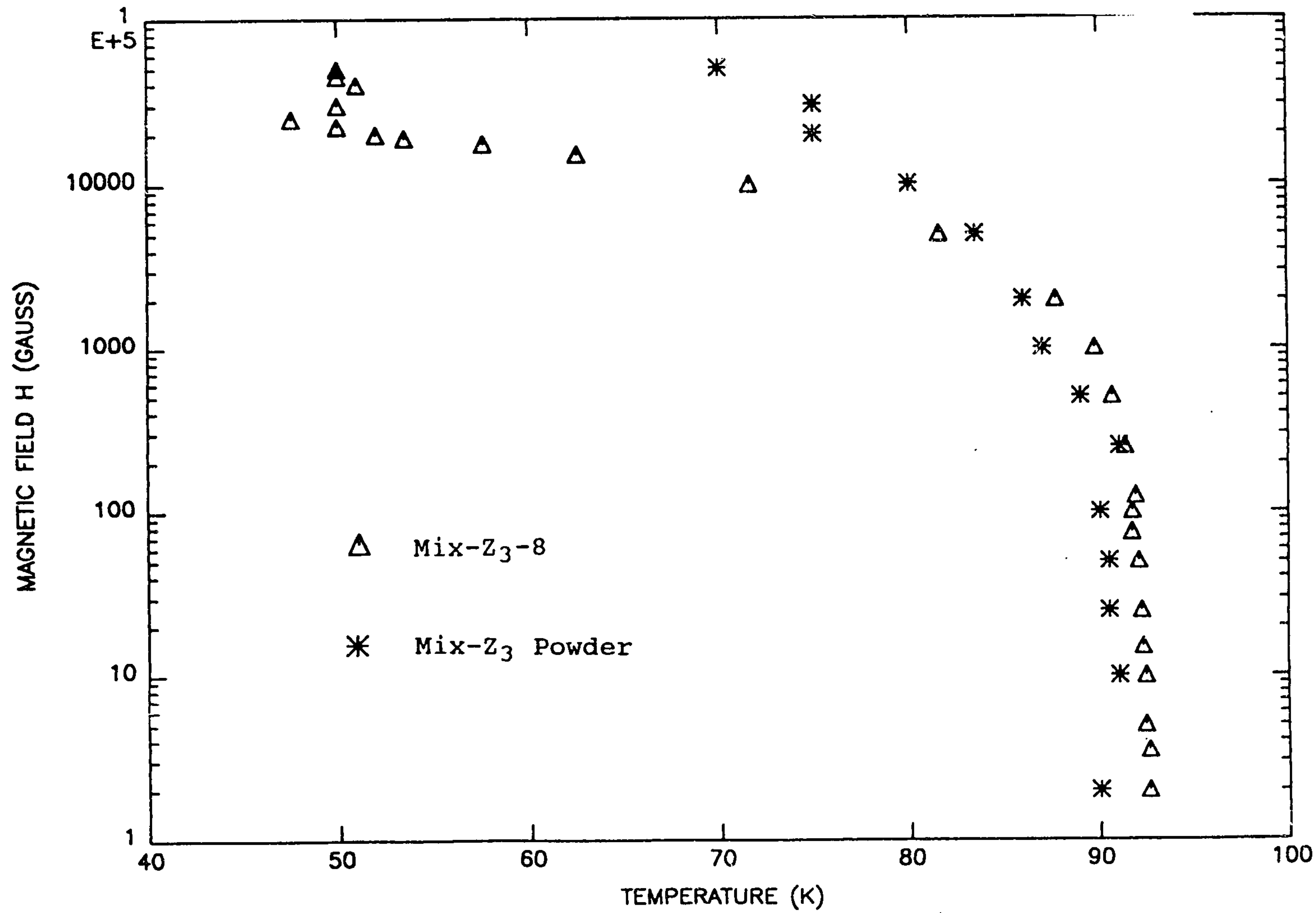

Fig 3.15. Comparison of T_{irr} for Mix-Z_3-8 & Mix-Z_3 powder

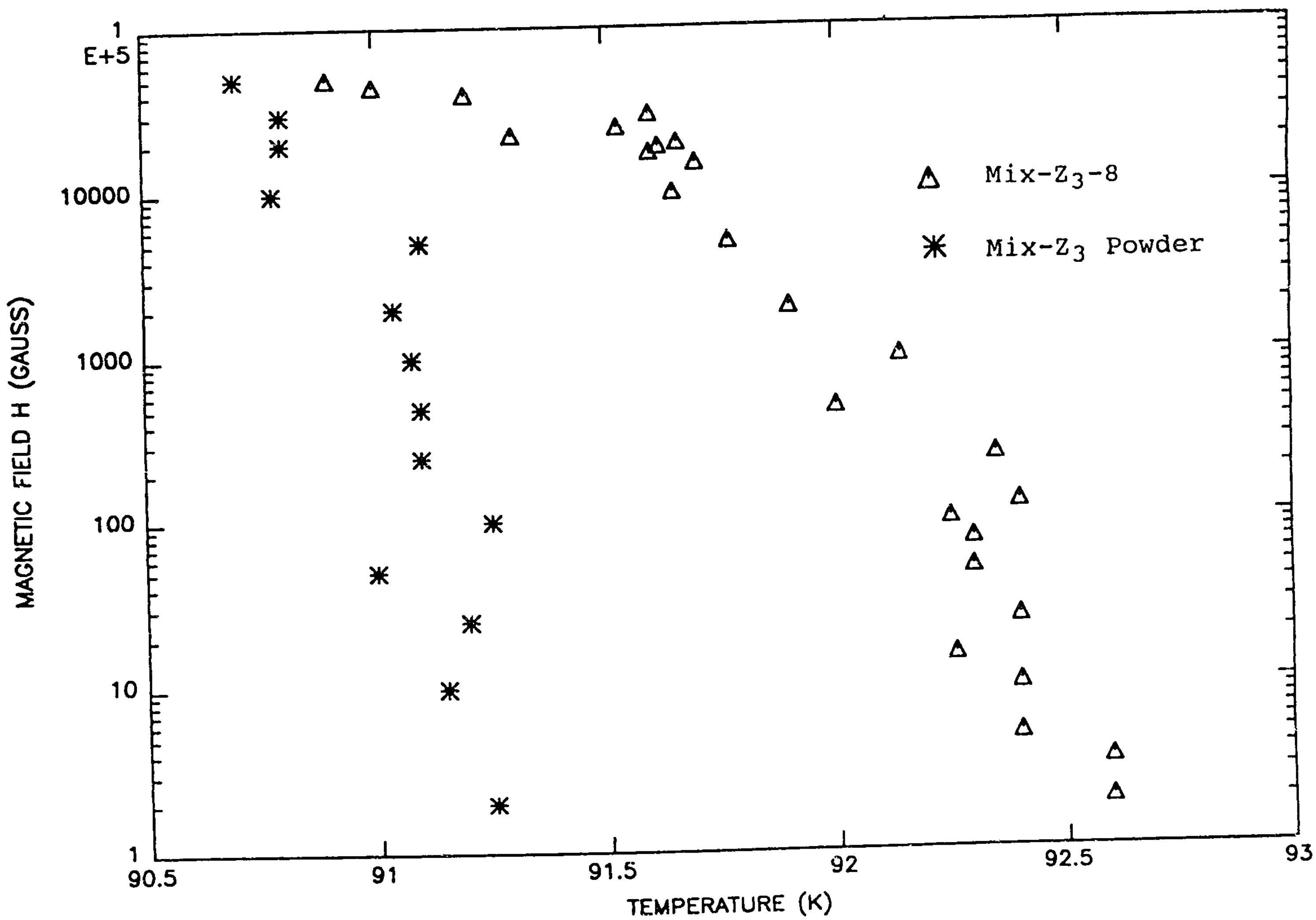

Fig 3.16. Comparison of Tc for Mix-Z_3 powder & Mix-Z_3-8

3.3.3. **Samples Mix-Z3-8 & Z3-8 (Van) Measurement Results**

Fig 3.9-3.11 are three of measurement results for the high pressure sample Mix-Z_3-8 We take similar analysis as in section 3.3.2. We get Table 3.6 for Mix-Z_3-8 and Table 3.7 for Mix-Z_3-8 (Van). Fig 3.12 shows the behavior of T_{irr}. For $H \leq 1$ Gauss, the results were measured by Prof. S. Gygax.

Fig 3.13 & 3.14 show the comparison of samples Mix-Z_3-8 (Van) & Mix-Z_3-8. For the behavior of T_c these two samples are similar. For the behavior of T_{irr}, at the low field they are similar, but at high field they are a little bit different. The T_{irr} of sample Mix-Z_3-8 is constant in high field region. The T_{irr} of sample Mix-Z_3-8 (Van) however shows a more gradual temperature dependence. So the reversibility behaviors in high field region seems to be sample dependent. Fig 3.15 & 3.16 show the comparison of samples Mix-Z_3-8 & Mix-Z_3 powder. The behaviors of T_{irr} for two samples are quite different. The T_{irr} of powder sample changes more rapidly than that of high pressure one. As for T_c , at low field, T_c of Mix-Z_3-8 is about 1 -- 1.4K higher than that of Mix-Z_3 powder.

TABLE 3.6 T_c, T_{irr}, of Mix-Z_3-8 high pressure sample

H (Gauss)	log H (log G)	T_{irr} (K)	T_c (K)
0.22	-0.66666	58.09	92.60
0.52	-0.28571	77.67	92.60
1	0.00000	81.90	92.60
2	0.30103	92.60	92.60
3.5	0.54407	92.60	92.60
5	0.69897	92.40	92.40
10	1.00000	92.40	92.40
15	1.17610	92.26	92.26
25	1.39794	92.20	92.40
50	1.69897	92.06	92.30
75	2.00000	91.68	92.30
100	1.87506	91.70	92.25
125	2.09691	91.87	92.40
250	2.39794	91.30	92.35
500	2.69897	90.65	92.00
1000	3.00000	89.75	92.14
2000	3.30103	87.72	91.90
5000	3.69897	81.6	91.77
10000	4.00000	71.6	91.65
15000	4.17609	62.5	91.70
17500	4.24304	57.6	91.60
19000	4.27875	53.5	91.62
20000	4.30103	52.0	91.66
22500	4.35218	50.0	91.30
25000	4.39794	47.6	91.53
30000	4.47712	50.0	91.60
40000	4.60206	51.0	91.20
45000	4.65321	50.0	91.00
50000	4.69897	50.0	90.90

TABLE 3.7 T_c, T_{irr} of Mix-Z_3-8 (Van) high pressure sample

H (Gauss)	log H (log G)	T_{irr} (K)	T_c (K)
5	0.30103	92.4	92.40
10	1.00000	92.0	92.28
25	1.39794	92.0	92.18
50	1.69897	91.5	92.15
100	2.00000	91.2	92.00
125	2.09691	91.5	92.12
250	2.39794	90.7	92.10
500	2.69897	90.0	92.10
1000	3.00000	89.5	92.08
2000	3.30103	88.0	92.00
5000	3.69897	80.4	92.00
10000	4.00000	71.4	91.82
20000	4.30103	60.8	91.80
30000	4.47712	55.0	91.80
50000	4.69897	45.0	91.50

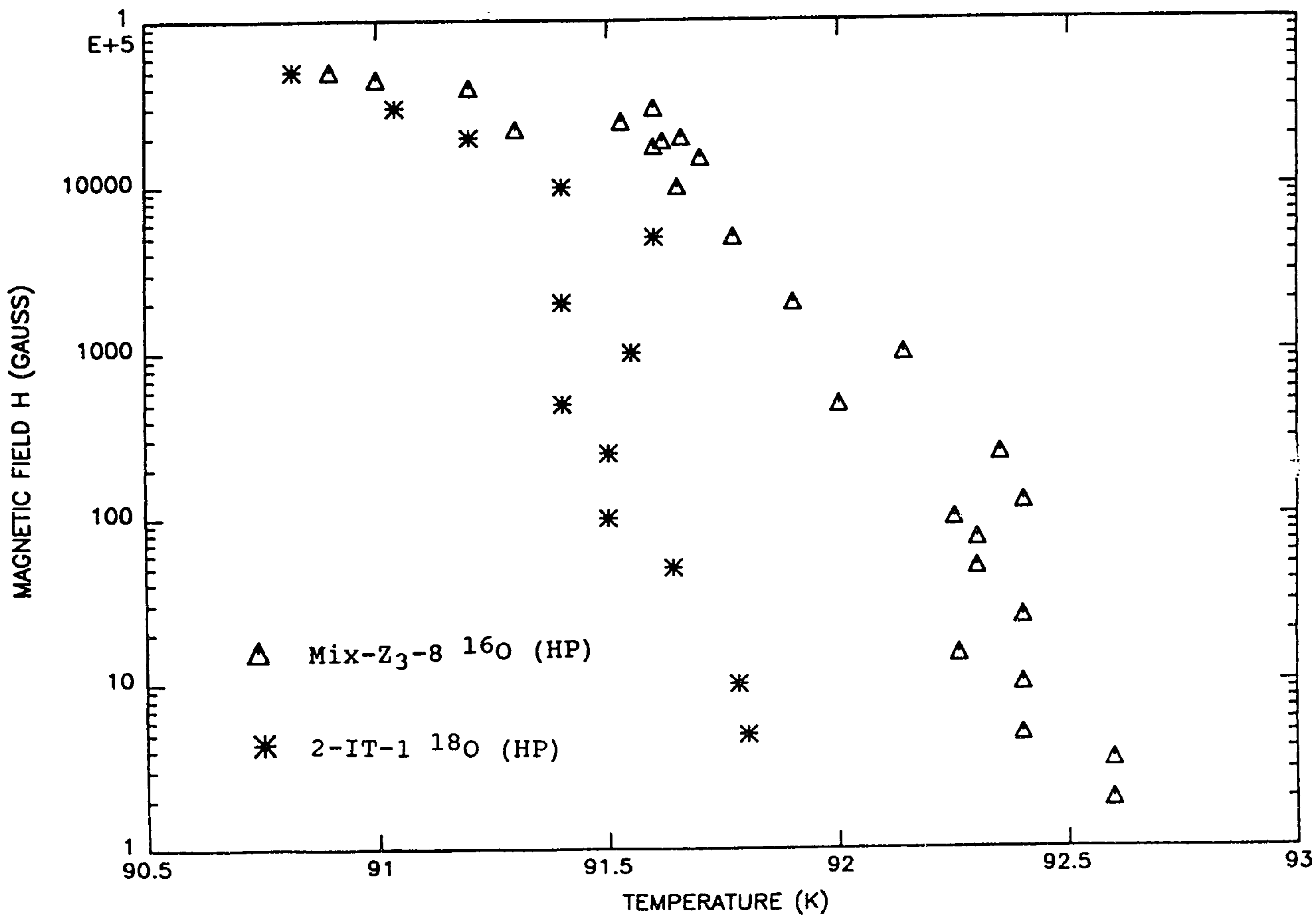

Fig 3.17. Comparison of Tc for 2-IT-1 ^{18}O (HP) & Mix-Z_3-8

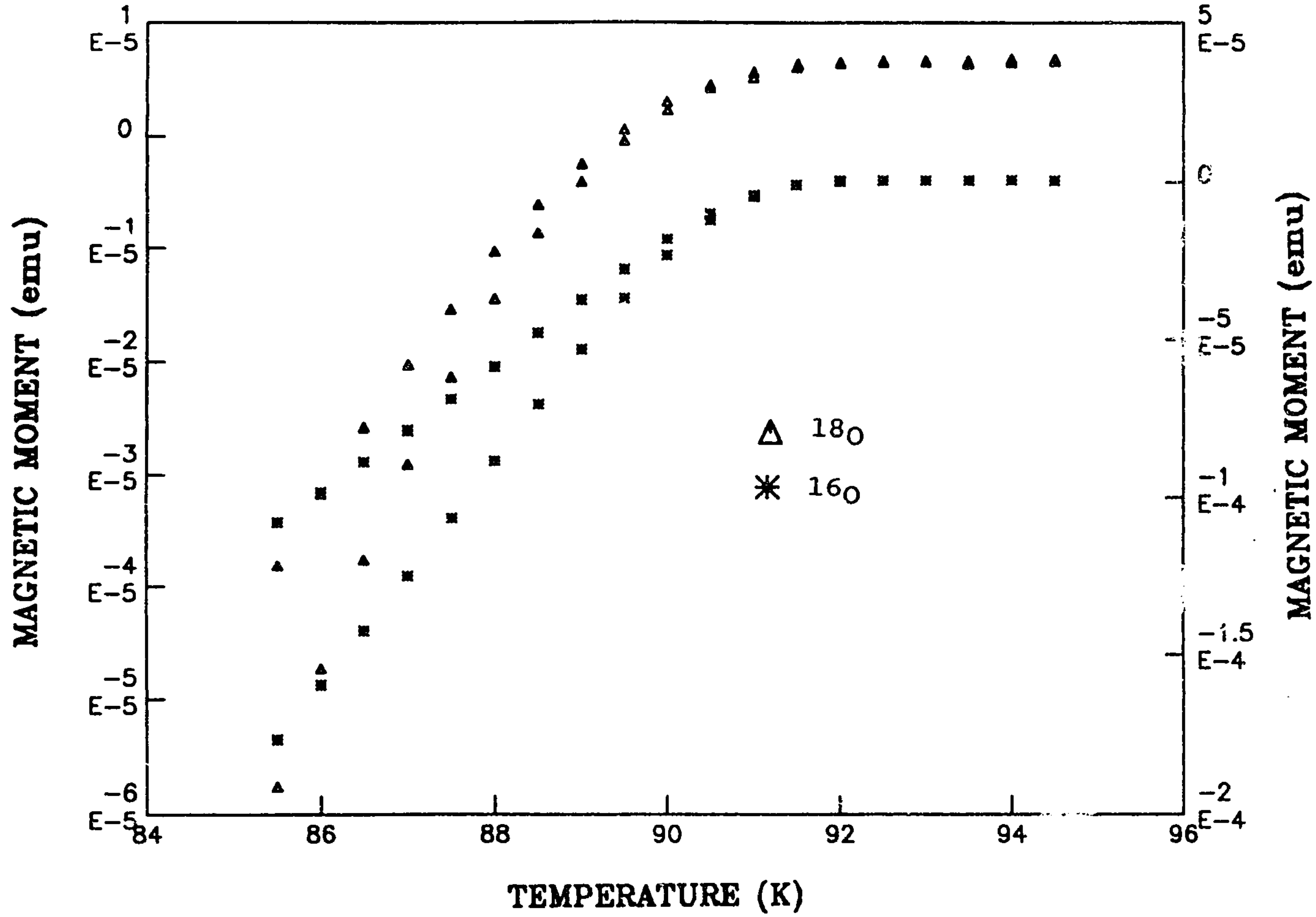

Fig 3.18. Comparison of Tc for 2-IT-1 ^{18}O (HP) and it reexchanged ^{16}O for ^{18}O at 500°C H=10 Gauss

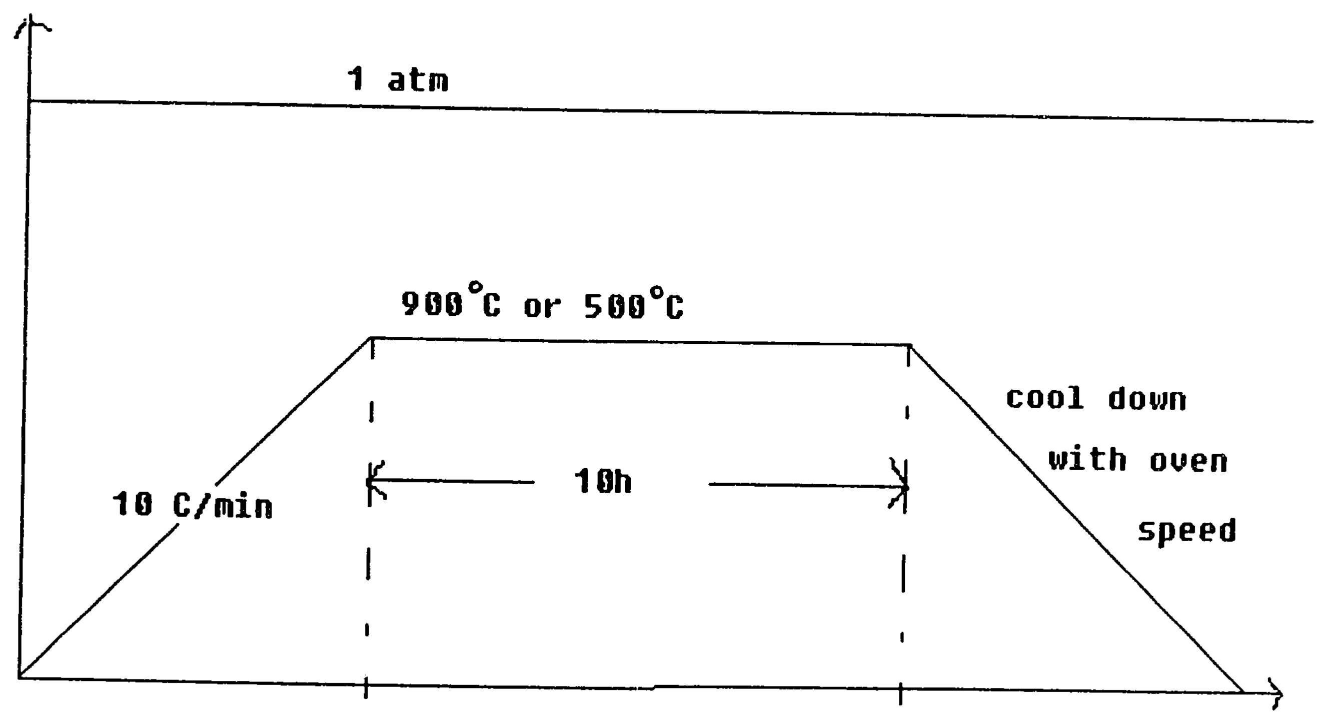

Fig 3.19. Reexchange ^{16}O for ^{18}O process at 900°C

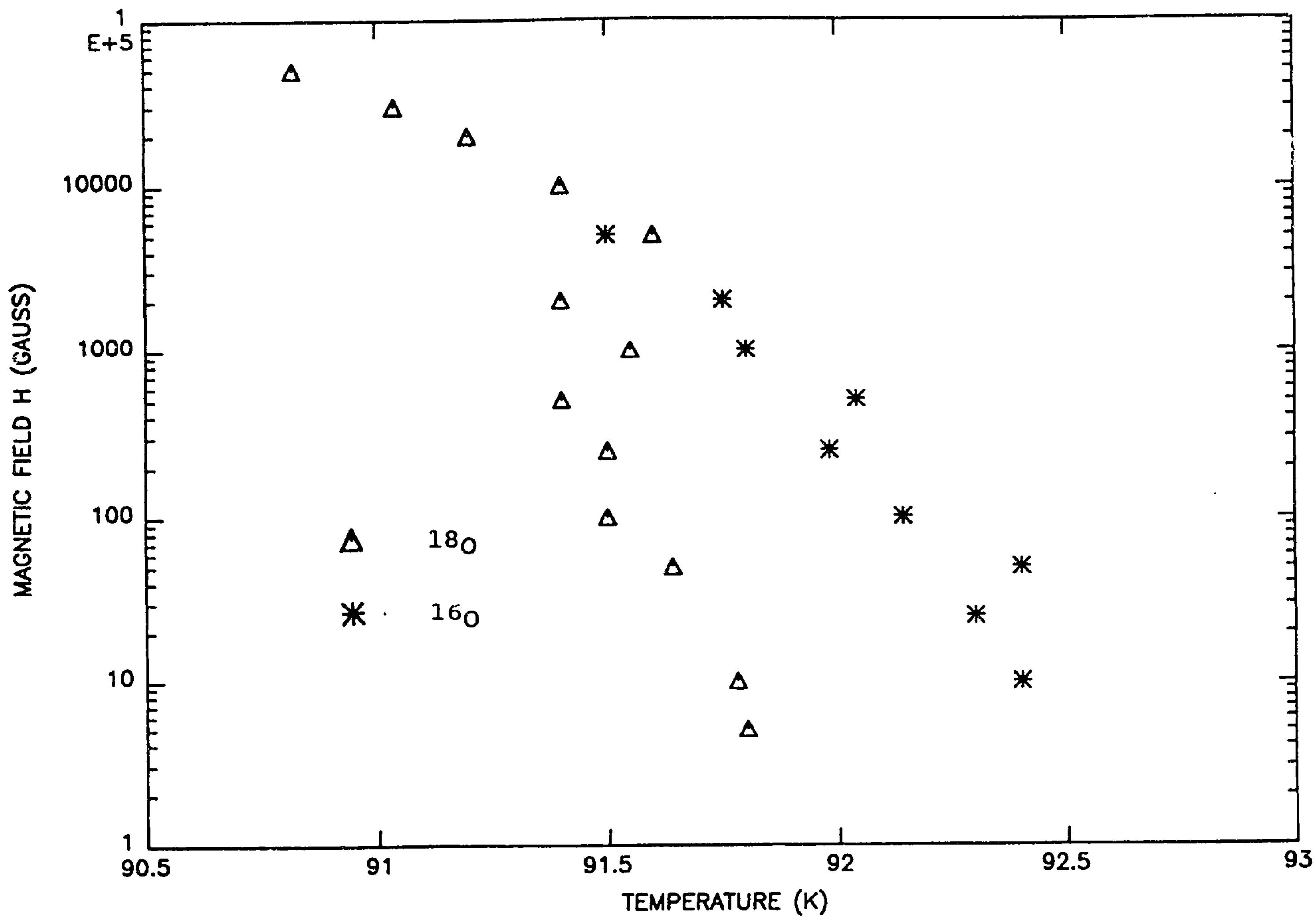

Fig 3.20. Comparison of T_c for resubstitution of ^{16}O for ^{18}O at 900°C

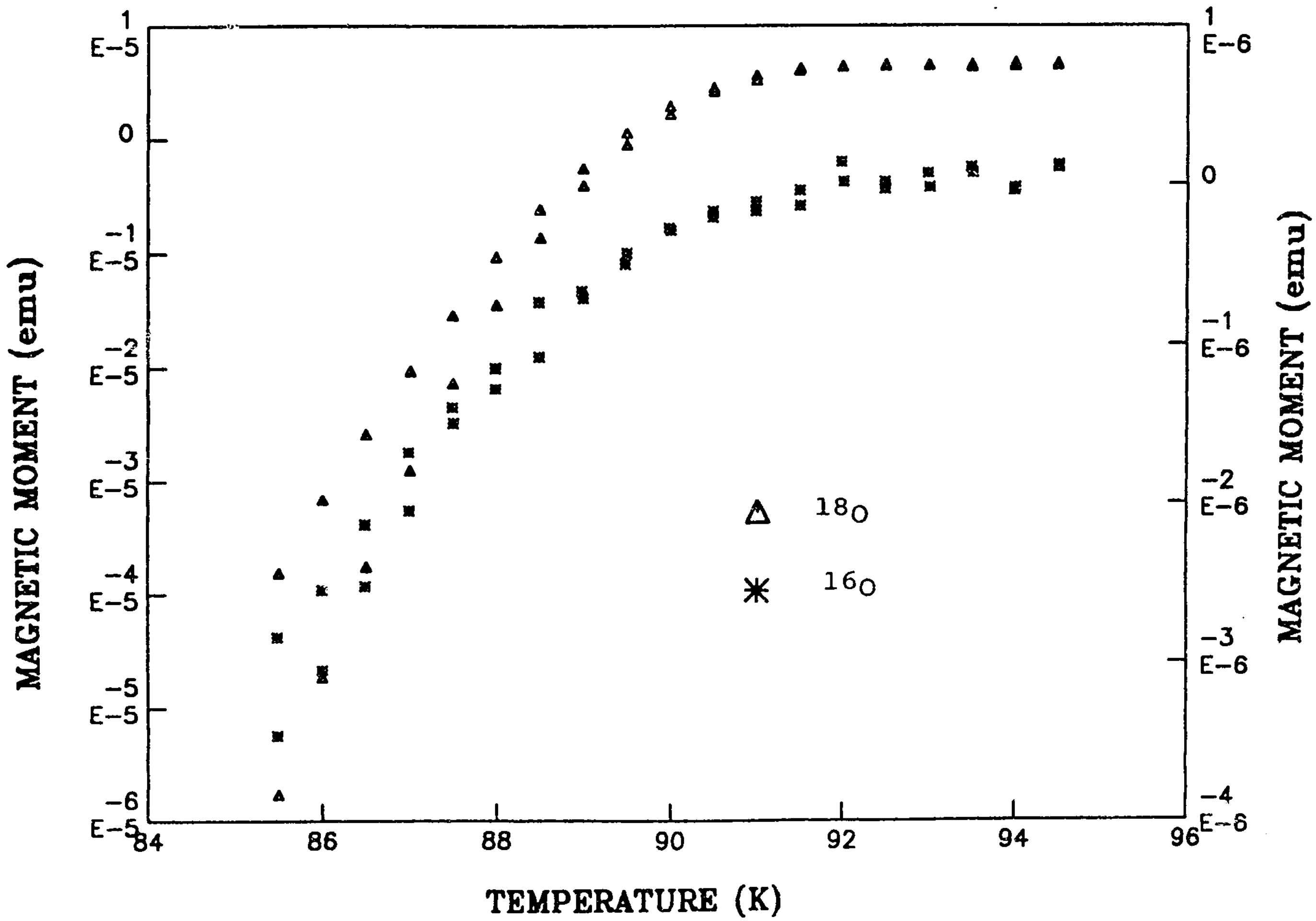

Fig 3.21. Comparison of Tc for 2-IT-1 ^{18}O (HP) and it reexchanged ^{16}O for ^{18}O at 900°C H=10 Gauss

3.3.4. The ^{18}O Substituted Samples

We use the Quantum Design SQUID magnetometer to measure T_c of 2-IT-1 ^{18}O (HP) at different fields. The result is shown in Table 3.8.

TABLE 3.8 T_c of sample 2-IT-1 ^{18}O (HP) for different field

H (Gauss)	log H (log Gauss)	T_c (K)
5	0.30103	91.80
10	1.00000	91.78
50	1.69897	91.64
100	2.00000	91.50
250	2.39794	91.50
500	2.69897	91.40
1000	3.00000	91.55
2000	3.30103	91.40
5000	3.69897	91.61
10000	4.00000	91.40
20000	4.30103	91.20
30000	4.47712	91.04
50000	4.69897	91.82

Fig 3.17 shows the comparison in T_c of 2-IT-1 ^{18}O (HP) and Mix-Z_3-8 samples. From Fig 3.17 we find there is a small decrease in T_c of about 0.6 K at low field. Now, if we reexchange ^{16}O for ^{18}O at 500°C under normal pressure, we found that T_c was not back up as shown in Fig 3.18. If we reexchange ^{16}O for ^{18}O at 900°C under normal pressure as shown in Fig 3.19, we found that T_c was back up about 0.6 K at low field. Fig 3.20 & 3.21 and Table 3.9 show the

results.

TABLE 3.9 T_c of sample 2-IT-1 ^{18}O exchanged by ^{16}O at 900°C under normal pressure for different field.

H (Gauss)	log H (log Gauss)	T_c (K)
5	0.30103	92.40
10	1.00000	92.30
50	1.69897	92.40
100	2.00000	92.14
250	2.39794	91.98
500	2.69897	92.04
1000	3.00000	91.80
2000	3.30103	91.75
5000	3.69897	91.50

This means that T_c is nonreversible by resubstitution of ^{16}O for ^{18}O at 500°C but reversible by resubstitution of ^{16}O for ^{18}O at 900°C under normal pressure.

3.4. Analysis of Magnetic Measurement

3.4.1.. The Ebner-Stroud Superconducting-glass Model

Ebner and Stroud [26] proposed a theory for the diamagnetic response of weakly linked superconducting clusters. In that model, superconducting grains, each small compared to a penetration depth, are weakly coupled into closed loops. These support screening supercurrents in response to an external magnetic field. In a magnetic field, a large cluster can support many supercurrent-carrying states of nearly equal energy, but energy barriers between these states tend to inhibit hops from one state to another at low temperatures. The picture is similar to that often proposed for spin glasses [27]. Applying their model, various spin-glass features are predicted. These include differences between dc and ac magnetic susceptibility, and between magnetic behavior resulting from cooling in a field and cooling in zero field.

The clusters of interest contain N superconducting grains embedded in a non-superconducting host. The ith grain is centered at $\vec{x}_i$ and has a complex energy gap $\psi_i = \Delta_i \exp(i\phi_i)$. The grains are weakly coupled via the host according to the Hamiltonian [28-30]

$$H = -\sum_{<ij>} J_{ij} \cos(\phi_i - \phi_j - A_{ij}) \qquad 3.1$$

Here J_{ij} is the coupling energy between grains i and j, and the phase factor A_{ij} is given by

$$A_{ij} = \frac{2\pi}{\Phi_0} \int_i^j \vec{A} \cdot d\vec{l} \qquad 3.2$$

In Eq. (3.2), $\Phi_0 = hc/2e$ is an elementary flux quantum, and the line integral is taken along a line joining the centers of grains i and j. We can calculate the magnetic moment for each cluster directly from the circulating supercurrents. Thus the moment μ of a cluster is

$$\vec{\mu} = \frac{1}{2c}\sum_{<ij>} <\overrightarrow{X_{ij}} \times I_{ij}\overrightarrow{x_{ij}}> \qquad 3.3$$

where $$I_{ij} = \frac{2eJ_{ij}}{h}\sin(\phi_i - \phi_j - A_{ij}) \qquad 3.4$$

is the Josephson current from grain i to grain j, $\overrightarrow{X_{ij}} = (\overrightarrow{x_i} + \overrightarrow{x_j})/2$ is the vector joining the origin to the position of the midpoint between grains i and j, and $\overrightarrow{x_{ij}} = \overrightarrow{x_j} - \overrightarrow{x_i}$ is the vector distance from grain i to grain j. The magnetic moment of a finite cluster, of course, does not depend on the choice of origin in this expression, and so Eq.(3.3) is completely unambiguous. The canonical average of an operator $\theta(\phi_1,\ldots,\phi_n)$, denoted $<\theta>$, such as that given in Eq.(3.3) is computed from the relation

$$<\theta> = \frac{1}{Z}\int \theta(\phi_1,\ldots,\phi_n)\left[\prod_i d\phi_i\right]\exp(-H/K_BT) \qquad 3.5$$

where $$Z = \int\left[\prod_i d\phi_i\right]\exp(-H/K_BT) \qquad 3.6$$

is the partition function.

The key to this model is "frustration", which means the fact that at finite fields, any cluster with closed loops cannot find a state which simultaneously minimizes all the bond energies. The frustration is produced by the phase factors A_{ij}, which make some of the bonds ferromagnetic (i.e. favoring equal phases ϕ_i and ϕ_j), some antiferromagnetic, and most favoring an angle between these extremes. As in more familiar frustrated systems (e.g. magnetic models), a large frustrated cluster, with many closed loops, can choose among numerous competing ground states with nearly equal energy. In a finite cluster, only one of these is the true ground state. But others will lie only a small energy above it. As the field is varied, the various levels will cross one another. The cluster must hop from one configuration to another in order to stay in the ground state. Each such hop will accompanied by an abrupt change in magnetization.

This picture leads to a difference between the dc and ac diamagnetic susceptibilities. These two are defined by the relation:

$$\chi_{ac} = \left[\frac{\partial M}{\partial H}\right]_T, \qquad \chi_{dc} = \left(\frac{M}{H}\right)_T \qquad 3.7$$

Here H is the external magnetic field, and M is the magnetic moment per unit volume. The χ_{dc} is a true equilibrium property. χ_{ac} can be measured by superimposing on a fixed dc field a small-amplitude parallel ac field. If the frequency is larger than the relaxation rate of cluster, χ_{ac} measures a nonequilibrium property. It is also typically larger than χ_{dc}. These differences are also characteristic of more usual spin glasses.

3.4.2. Morgenstern-Muller-Bednorz Superconducting Glass Model

Morgenstern, Muller, and Bednorz [32] presented a numerical simulation for an XY-spin-glass model. They outlined the connection to the experiments on high T_C superconductors, provided a phase diagram which is important for future experiments, and particularly they reproduced the glass behavior in experiments by a 2-D model. They also predicted a substantial gain in T_C for enhanced couplings between planes.

The following is a brief review of the model. Consider an array of N superconducting clusters coupled by Josephson tunnelling. A cluster is defined as a region of coherent phases in the superconductor. This definition is more general than in usual models for granular superconductors, where only arrays of (physical) grains are considered. This model allows clusters inside these physical grains, in contrast to Ebner and Stroud [26] and John and Lubensky [33]. The ith cluster is located at $\vec{x}_i$ and has a complex energy gap $\psi_i = \Delta_i \exp(i\phi_i)$ (3.8). The system is then described by an XY-(spin-glass) Hamiltonian

$$-\beta H = \sum_{<i,j>} J_{ij} \cos(\phi_i - \phi_j - A_{ij}) \qquad 3.9$$

where $\beta = 1/KT$, and the J_{ij} s are the coupling energies between domains of uniform phases i and j. Following Ebner and Stroud, they consider the case $J_{ij} = J$ for nearest neighbors only and otherwise zero. Because we concentrate on glassy behavior, the change of the J_{ij} 's does not lead to any frustration effects [34] and therefore they can be treated as constants.

On the other hand, frustration in Hamiltonian (3.9) arises from the phase factors A_{ij} as given in Eq.(3.2). The authors consider the two-dimensional (2-D) case for site disorder. Site disorder is introduced in the following way: They allow weak displacement of sites at their position of original square lattice (2-D case), i.e. within a radius r the new position is chosen randomly. We should mention especially a Gaussian distribution for the A_{ij} 's. The important point is that the site disorder enters via the vector potential $\vec{A}$, and leads to the frustration effects in the Hamiltonian. Applying a magnetic field in the z-direction $\vec{H}=(0 \;\; 0 \;\; H)$ (3.10) we have for the vector potential

$$\vec{H}=\nabla\times\vec{A} \quad ,\vec{A} = (\ 0,\ Hx,\ 0) \qquad 3.11$$

leading to

$$A_{ij}=\frac{2\pi}{\Phi_0}H\frac{x_i+x_j}{2}(y_j-y_i) \qquad 3.12$$

where x_i, y_i are the actual coordinates of the ith cluster, and Φ_0 is elementary flux quantum. As we have the term ($x_i + x_j$) in (3.12), the A_{ij} 's increase in some corner of the lattice. This type of disorder seems to be essential for the behavior of superconducting glasses.

It is important to note that the present model can be derived without using the BCS theory. Any mechanism leading to Superconductivity inside the clusters will result in the model described here.

There are several limitations of the model. The first point is that the J_{ij}'s are kept constant and couple only nearest neighbors. They might also depend on T and H. But as pointed out, they neither play a role for frustration effects, nor, therefore, the spin-glass behavior. The second point is that the present model is certainly limited to the case where the London penetration depth is large compared to cluster size and their separation, where we can set local field equals applied field. The third point is that the line integral in the definition of the phase factors A_{ij} has to be replaced by a suitable average for wider junctions. The last but important question considers the dimensionality of the system. Here, they deal with 2-D lattices mainly because of technical reasons. A qualitatively acceptable description of the experiments by their 2-D calculations supports the 2-D layer picture found for single crystals [37].

A. De Almeida-Thouless Line

The most surprising finding in the experiments of Muller et al.[25] was the existence of a quasi-de Almeida-Thouless (AT) line separating equilibrium from metastable behavior in the susceptibility for different magnetic fields, they obtain $H^{2/3} \propto T_c(0) - T(H)$ (3.13). Here T(H) denotes the temperature where equilibrium and metastable susceptibilities start to differ or, more generally, where irreversible effects start to occur.

This behavior is well known in spin glasses. A similar

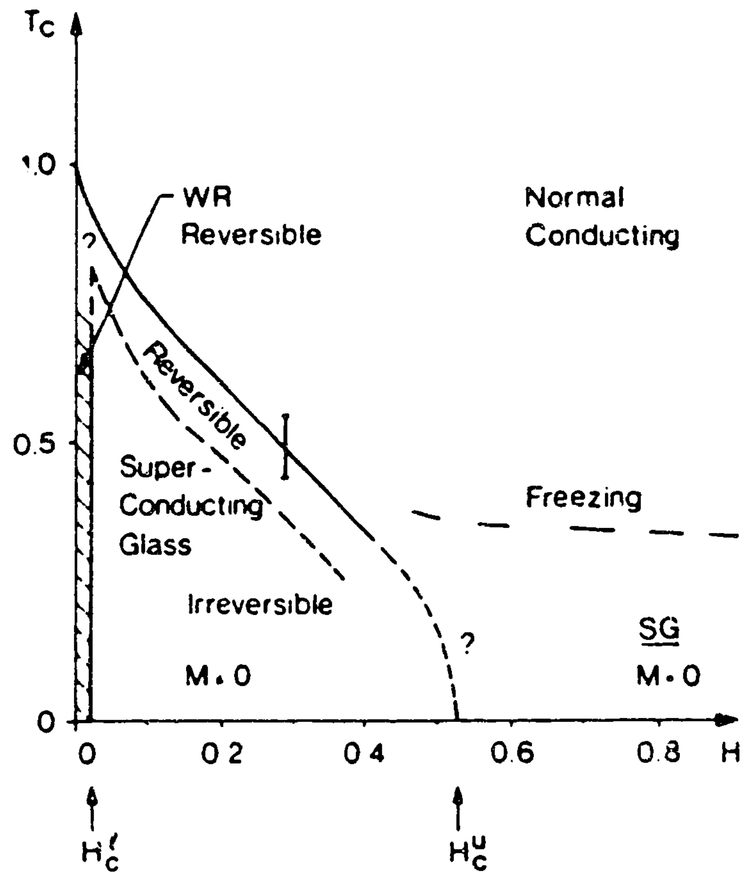

Fig 3.22. Phase diagram in H-T plane. Reversible weak-random (WR) phase between $H = 0.0$ and $H_c^l = 0.01 - 0.03$. Between H_c^l and $H_c^u = 0.5$, superconducting-glass phase. Irreversible effects are separated from reversible effects by dashed line. Above H_c^u, usual XY-spin-glass phase (SG). Dashed line indicates freezing transition. (after Morgenstern et al. [32])

line separating metastable from stable regions in the H-T plane was originally obtained by de Almeida and Thouless [35]. But one substantial difference has to be noted: They consider the famous Sherrington-Kirkpatrick model [36] in applied magnetic field:

$$-\beta H = \sum_{ij} J_{ij} S_i S_j + H \sum S_i \qquad 3.14$$

where the J_{ij}'s are Gaussian-distributed random couplings between all (Ising) spins (mean field limit). The magnetic field couples directly to a spin. In the superconducting-glass situation, the magnetic field enters via vector potential $\vec{A}$ and phase factors A_{ij}; leading to an increase of disorder and frustration which in the spin-glass models is introduced by the random distribution of the couplings J_{ij}. Therefore, the nature and origin of the "quasi" AT line are substantially different from the spin-glass case. Nonetheless, in their numerical work, Morgenstern et al. still found "quasi" AT lines; but the physical interpretation of the original spin-glass theories is not valid.

B. Phase Diagram

According to the numerical simulation results of Morgenstern et al.[32], they propose a phase diagram in the H-T plane as shown in Fig 3.22. Applying a small field, we do not enter the superconducting-glass phase immediately. There exists a small critical field H_c^1 which marks the breakdown of the weak-random (WR) phase. In the WR phase, we have ("almost") reversible effects.

For fields larger than H_c', we enter the superconducting-glass phase which is separated from the paramagnertic or normal conducting phase by a line that is proportional to $H^{2/3}$ or, better the exponent is relatively close to 2/3. The $H^{2/3}$ behavior breaks down at fields of values somewhat higher than H=0.4 (in experimental unit, this means H=8k Gauss). The dotted line indicates the uncertainty of the phase boundary; here we clearly see irreversible effects. The dashed line in Fig 3.22 denotes $T^*(H)$ above which we again have reversible effects.

For higher fields, $H \geq 0.5$ (experimental unit H=1 T), we conclude to find "pure" spin-glass behavior, but as a metastable, i.e. freezing effect (frozen in equilibrium). In equilibrium, we have M=0. The horizontal dashed line indicates the observation-time dependent freezing temperature.

The essential findings of the phase diagram: The quasi-AT line as found in experiments can be explained as the phase boundary between the superconducting-glass phase and the normal-superconducting regime. This phase boundary scales with $H^{2/3}$. But the mechanism for the decrease of T(H) is therefore quite different from the AT behavior in the Sherrington-Kirkpatrick (SK) model. While we have increasing disorder and therefore increasing frustration leading to a lower $T_c(H)$ when H is increased, we have the suppression of metastable states in the spin-glass phase as a consequence

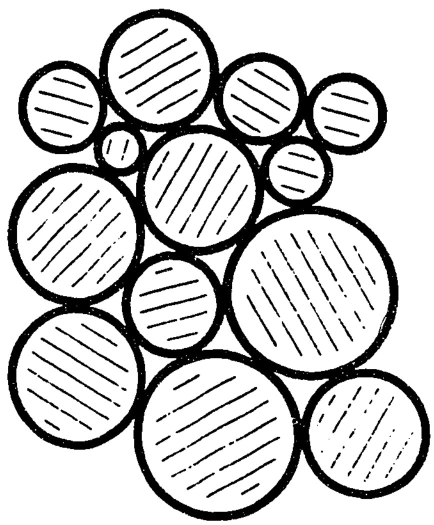

Fig 3.23. Model of ceramic layers of 2-D planes inside physical grains (random directions!) (after Morgenstern et al.[32])

of the applied field. Furthermore in contrast to the SK model we have a transition temperature T(H) (full line in Fig3.22) where we enter the superconducting glass phase, and a lower temperature $T^*(H)$ (dashed line) where reversible and irreversible behaviors in the glass phase start to differ. In the SK model, these two temperatures (T(H) and $T^*(H)$) are the same.

C. Model for Ceramic

As Morgenstern et al. have pointed out, it is very likely that the clusters of coherent phases are situated inside the physical grains as already mentioned in [26]. The 2-D nature of the model is supported not only by experiments on single crystals [37], but also by numerical work. The weak site randomness in the model cannot originate from the amorphous structure of the ceramic or powder. Weak disorder is certainly more likely inside the physical grains. Therefore, the regions of coherent phases are much smaller than the physical grains. Furthermore, their preliminary 3-D simulations have shown different behavior than 2-D. This supports the 2-D model which is closer to experiments, and additionally is in agreement with coherent phases inside the physical grains. Thus, we have inside each physical grain layers of decoupled (or very weakly coupled) planes of the 2-D XY-spin-glass model. The direction of these layers in the whole ceramic is therefore distributed randomly. A schematic picture is given in Fig 3.23.

An important fact which is crucial for the understanding of glass properties and the proposed model is the size of the coherence length ξ. ξ is relatively small compared to ordinary superconductors. Therefore,the size of the clusters in the model (i.e. the regions of coherent phases ϕ_i, not the physical grains) is relatively small, substantially smaller than the physical grains. Therefore, the glass behavior is also found in single crystals. The smallness of the coherence length is essential for the glass behavior and the difference to ordinary superconductors.

3.4.3. **Comparison With Our Results**

A. The Difference Between ZFC and FC

In the experiments, we see there is always difference between ZFC and FC except at very low external filed (<0.1 Gauss). Superconducting-glass model provides explanation for the difference between field-cooled and zero-field-cooled moment. If the clusters are cooled slowly in a fixed field. the resulting configuration should be in equilibrium because the slow cooling allows the cluster to be annealed at relatively high temperatures. Cooling in zero field, and turning on the field at fixed low temperature, may result in a metastable magnetization, since the cluster has no time to equilibrate as the field is turned on. This distinction between field cooling and zero-field cooling has often been noted in bulk spin glasses [31]. Similarly, if the clusters are field-cooled to a low temperature and the field is

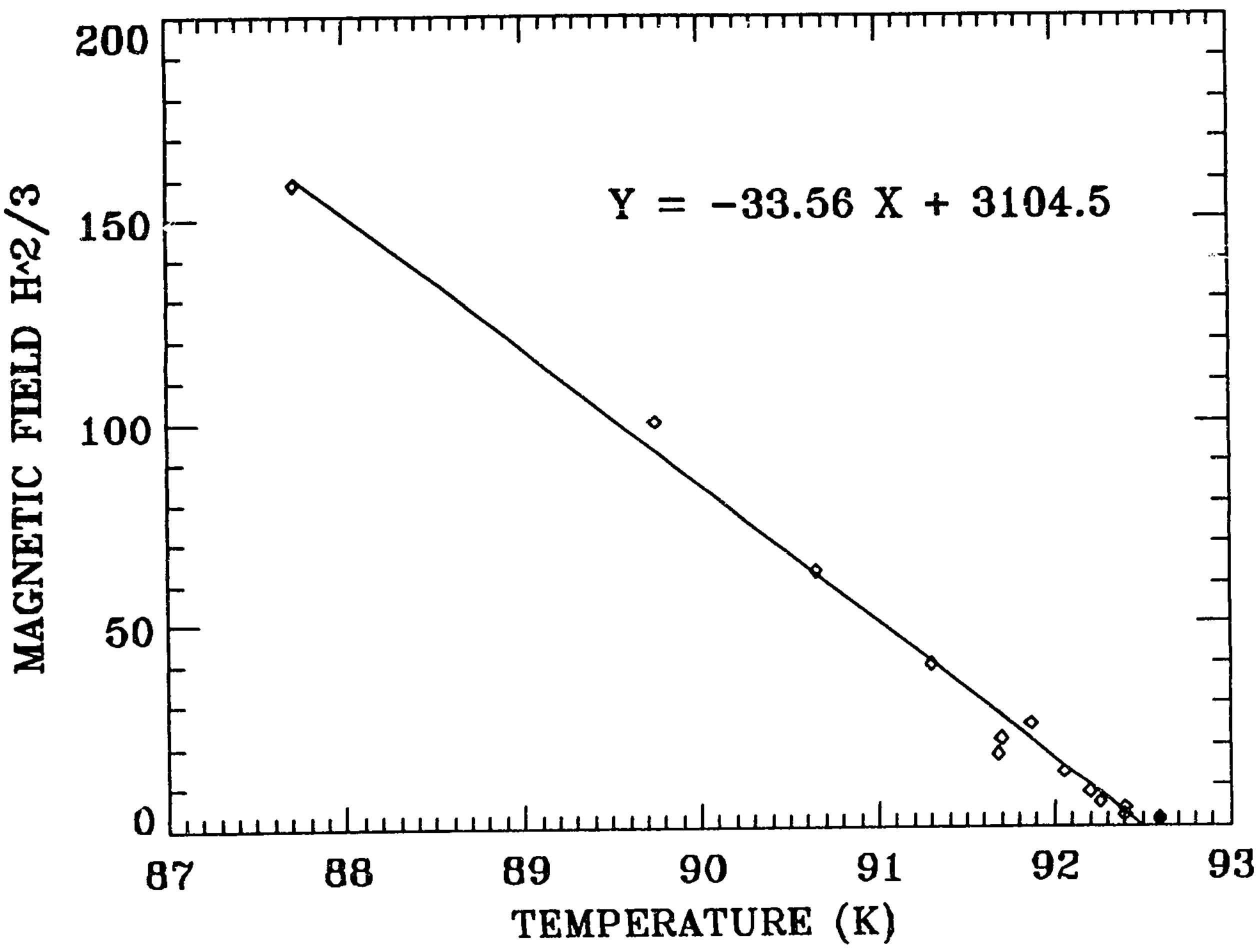

Fig 3.24. $H^{2/3}$ vs T_{irr} for high pressure sample Mix-Z_3-8

suddenly turned off, there will remain trapped flux which slowly decays away as the cluster equilibrates. This trapped flux is the superconducting analog of remanence in magnetic systems. Its decay should have an anomalous (i.e. nonexponential) time dependence characteristic of a very broad distribution of relaxation times, just as is seen in true spin glasses.

B. De Almeida-Thouless Line

Now, I plot $H^{2/3}$ vs T_{irr}. We try to find whether our samples satisfied Eq.(3.13). Fig 3.24 shows the results for high pressure sample Mix-Z_3-8. From the graphics, we see in the region H ≤Gauss, we have "quasi-de Almeida- Thouless" line.

$$H = 1 \ldots \left[\quad \frac{T}{\cdot 2.5} \right]^{\frac{3}{2}} \; (T) \qquad 3.16$$

Th[illegible]ult for high pressure sample is quite different from the results mentioned in [44] that an irreversibility line which follows a (1 - T/T_c) ∝ $H^{2/3}$ law all the way to 20 T.

Because the effective area occupied by a flux quantum is given roughly by

$$S_{eff} \approx \frac{\Phi_0}{H} \qquad 3.17$$

where $\Phi_0 - 2\times10^{-7} G.cm^2$, we can estimate the loop size in Eq.(3.16). For an applied field of H~2000 Gauss, $\Phi_0 - 2\times10^{-7} G\ cm^2$

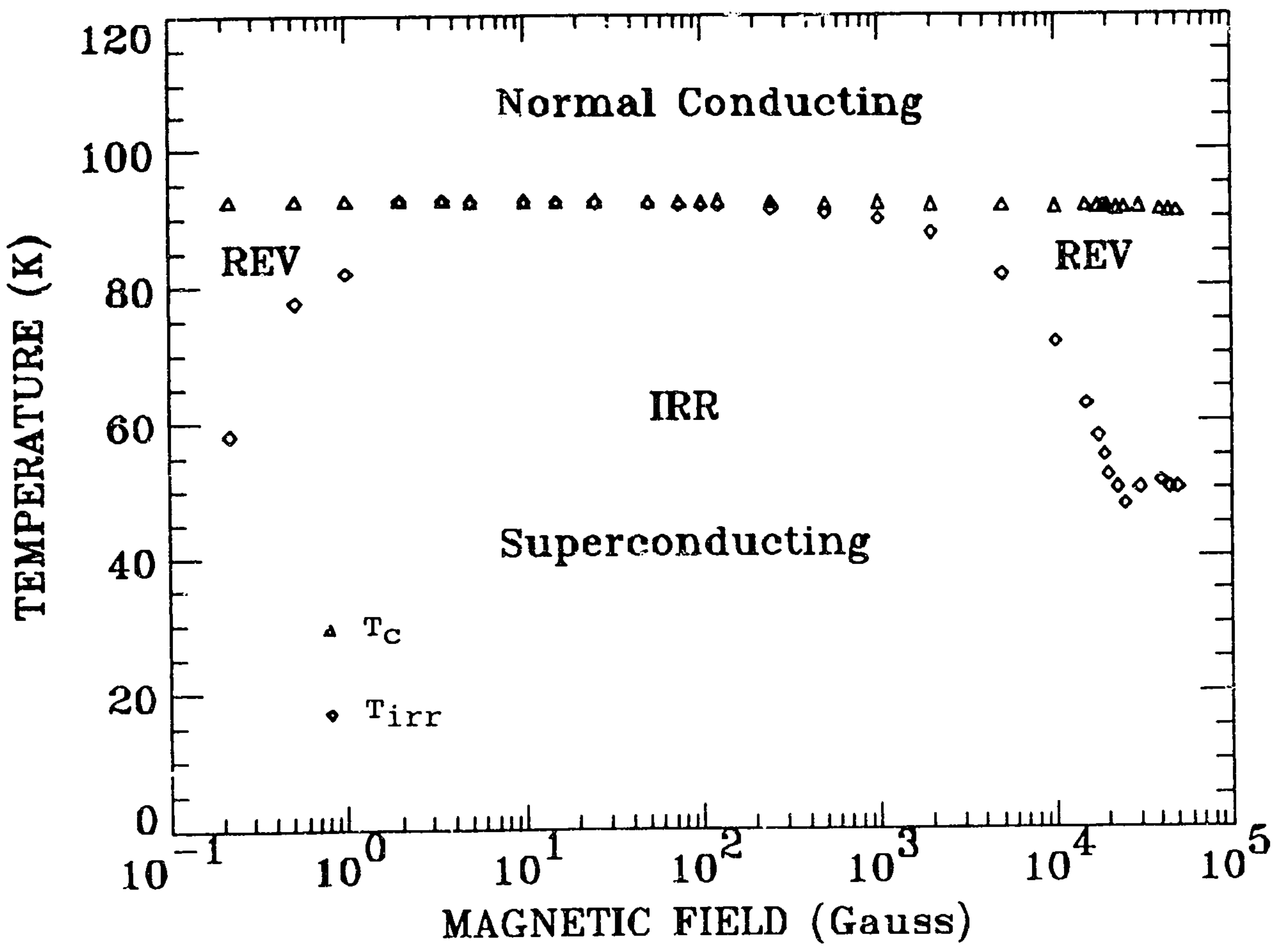

Fig 3.25. Phase Diagram for Mix-Z_3-8

, we get $S_{eff} = 10^{-10}$ cm^2. So the loop size is in order of 1000 A, which is about the order of twin spacings. This result is also quite different from the argument in [38], that if an irreversibility line which follows a $(1 - T/T_c)$ ∝ $H^{2/3}$ law all the way to 20 T, then it requires the loop size in Eq.(3.16) to be less than 100 A, which is implausibly small for twin spacings.

C. Phase Diagram

Now if I plot T_c vs H and T_{irr} vs H on the same graph, we get the magnetic phase diagram as shown in Fig 3.25. The line separating the superconducting from the normal conducting phase is the T_c line. The curve separating reversible from irreversible region is T_{irr}. Only for 1 Gauss < H < 2k Gauss does T_{irr} satisfy $H^{2/3} \propto [T_c(H) - T_{irr}(H)]$. Also from Fig 3.25, we can see for H < 0.2 Gauss, the reversible effects, which correspond to the weak-random phase (WR) in Fig 3.22; for H > 0.2 Gauss, we enter the irreversible region corresponding to the superconducting-glass phase.

In conclusion, we get the magnetic phase diagram similar to Fig 3.22, but not the same.

These facts might suggest that the high pressure samples may give some support to the superconducting-glass model.

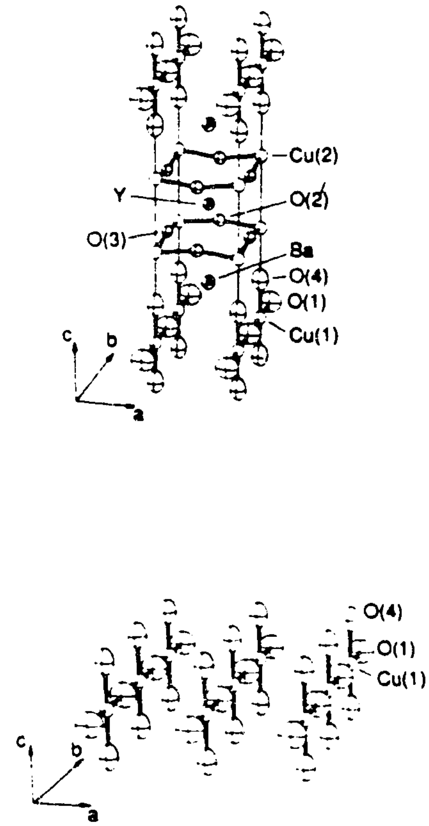
Cu(2)
Y
O(2)
O(3)
Ba
O(4)
O(1)
Cu(1)
c
b
a
O(4)
O(1)
Cu(1)
c
b
a

(a)

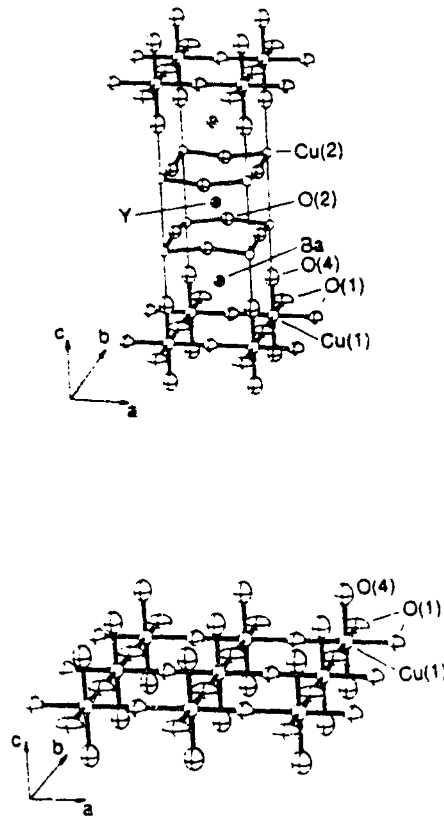
Cu(2)
Y
O(2)
Ba
O(4)
O(1)
Cu(1)
c
b
a
O(4)
O(1)
Cu(1)
c
b
a

(b)

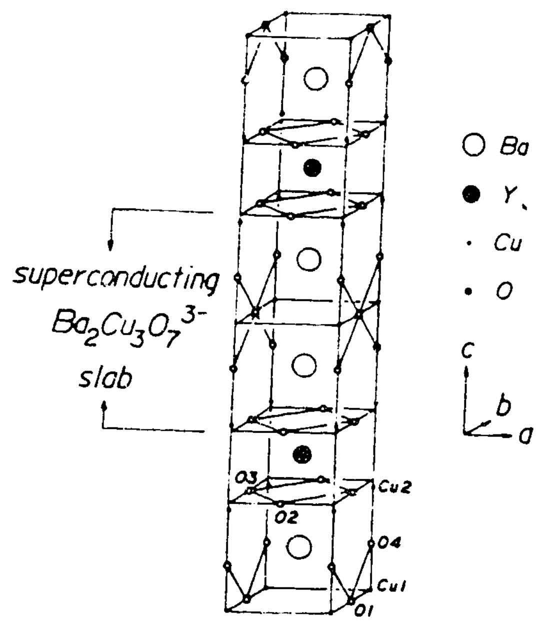

(c)

Fig 3.26. Crystal structure of $Y_1Ba_2Cu_3O_{7-\delta}$. (a) The orthorhombic Pmmm phase. Orthorhombic phase exhibiting complete ordering of oxygen atoms onto the (0, 1/2, 0) site which results in one-dimensional CuO3 chains along the b axis. (b) The tetragonal P4/mmm phase. Tetragonal phase showing a disordering of the oxygen atoms in the z=0 plane. (after Jorgensen et al.[67]). (c) slab Fig. (after Beno et al.[39]).

3.5. **Analysis of Measurements on ^{18}O Substituted Samples**

3.5.1. **The Transition Temperature**

A. The Normal High Pressure Sample

From Fig 3.16, we see that at low fields, the T_c of the high pressure sample is about 1 to 1.4K higher than that of the normal pressure sample. At high field the two curves are approaching.

B. The Isotope High Pressure Sample

From the Figs 3.17, 3.18, 3.20, and 3.21, we could see there is a small decrease in T_c of about 0.6K when ^{16}O is substituted by ^{18}O for high pressure sample, and the shift is nonreversible by resubstitution of ^{16}O for ^{18}O at 500°C but is reversible by resubstitution of ^{16}O for ^{18}O at 900°C.

3.5.2. **The Oxygen Concentration Model**

The high T_c (T_c > 90K) superconductor $Y_1Ba_2Cu_3O_{7-\delta}$ as determined by powder neutron diffraction studies [45-48], has an orthorhombic structure as shown in Fig 3.26(c). Substitution of Y^{3+} by lanthanide ions Ln^{3+} (e.g. Ln=Sm, En, Gd, Dy, Ho, Yb) hardly affects the high temperature superconductivity [43,44], so the structural unit essential for the high-temperature superconductivity is the two-dimensional (2D) $Ba_2Cu_3O_{7-\delta}^{3-}$ slab [45]. The ideal stoichiometry $Y_1Ba_2Cu_3O_7$ is possible when all the oxygen sites of Fig 3.26(c) are fully occupied. A stoichiometric $Ba_2Cu_3O_7^{3-}$ slab consists of two CuO_2 layers that sandwich one CuO_3 chain and two Ba atoms per unit cell. The copper atom coordination is "square planar" for the CuO_3 chains, and is "square pyramidal" for the CuO_2 layers. The O(4) atoms of the CuO_3 chains occupy the apical positions of the Cu(2) atom "square pyramids", so the Cu(2) atoms of one CuO_2 layer are linked to those of the other CuO_2 layer via the O(4)-Cu(1)-O(4) bridges of the CuO_3 chains [45,46].

The oxygen atom vacancies of orthorhombic $Y_1Ba_2Cu_3O_{7-\delta}(\delta < 0.5)$ occur primarily at the O(1) positions of the CuO_3 chains, i.e. the (0, 1/2, 0) sites of Fig 3.26 [39-42]. Upon increasing temperature, the orthorhombic phase gradually loses its oxygen contents of the Cu(1) atom plane, and undergoes a phase transition to a tetragonal structure as δ increases beyond 0.5 [47,48]. In tetragonal $Y_1Ba_2Cu_3O_{7-\delta}(\delta > 0.5)$, both the (1/2, 0, 0) and (0, 1/2, 0) sites are occupied by oxygen atoms with a site population less than 0.25, so the tetragonal phase no longer has the CuO_3 chains. With increasing temperature, the tetragonal phase gradually loses its oxygen concentration of the Cu(1) atom plane eventually leading to the stoichiometry $Y_1Ba_2Cu_3O_6$ [47,48], which has no oxygen atoms in the Cu(1) atom plane. The superconducting transition temperature T_c of $Y_1Ba_2Cu_3O_{7-\delta}(\delta < 0.5)$ decreases with increasing δ, and reaches zero beyond $\delta > 0.5$ [50,51]. Therefore, the CuO_3 chains are crucial for the high-temperature superconductivity in $Y_1Ba_2Cu_3O_{7-\delta}$.

The superconducting transition temperature T_c does not

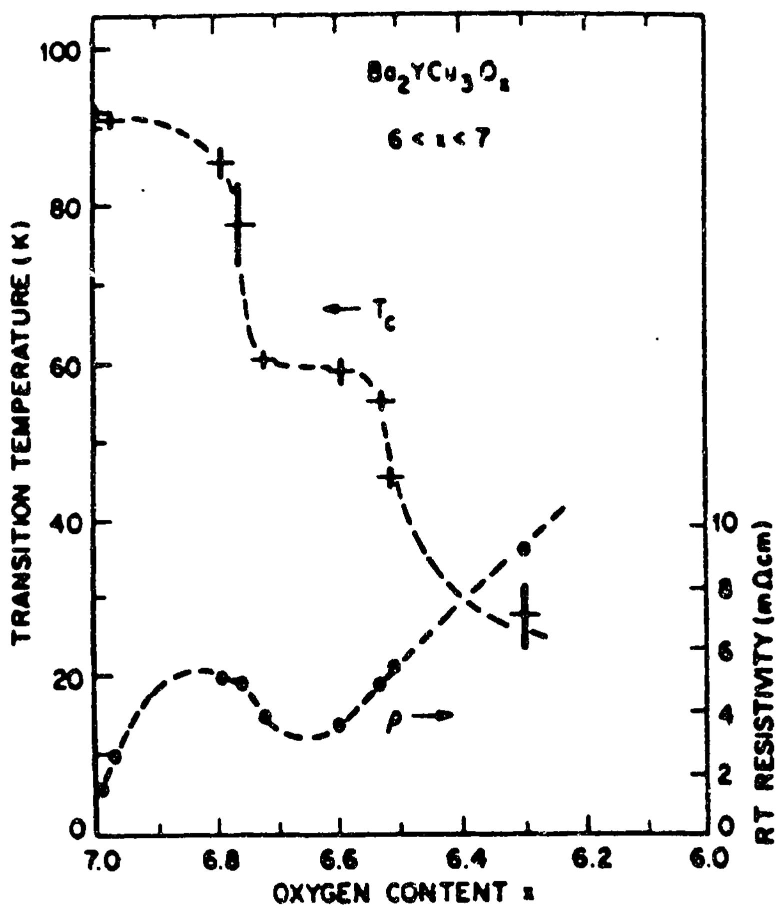

Fig 3.27. Oxygen content dependence of the resistive superconducting transition temperature in $Y_1Ba_2Cu_3O_x for 6.3 \leq x \leq 7$. (after Cava et al.[49]).

vary smoothly with oxygen concentration. Cava et al.[49] have shown that T_C varies stepwise from near 90K at $O_{6.96}$ to about 60K in the vicinity of $O_{6.67}$ and to a lower temperature ($T_c \doteq 20K$) below $O_{6.5}$ as shown in Fig 3.27. Moreover, the transitions are sharp and the room-temperature resistivity is lower in the center of a plateau region; the transitions are broad at intermediate compositions. These data clearly indicate the presence of some additional ordering not readily detectable with neutron or X-ray diffraction. The stepwise behavior depends on making conditions, Jorgensen et al. obtained a more general variation [67].

In almost all $Y_1Ba_2Cu_3O_{7-\delta}$ samples the oxygen atom vacancies occur primarily in the Cu(1) atom plane, so that a change in the overall oxygen concentration, $7-\delta$, is nearly identical to that in the oxygen concentration of the Cu(1) atom plane, $1-\delta$. Therefore, what really controls the magnitude of T_C in $Y_1Ba_2Cu_3O_{7-\delta}$ is not the overall oxygen concentration but the oxygen concentration of the Cu(1) atom plane. The latter controls the length of the Cu(2)-O(4)-Cu(1)-O(4)-Cu(2) linkage and hence the magnitude of interlayer interaction that occur via the Cu(2)-O(4)-Cu(1)-O(4)-Cu(2) linkages [52].

The oxygen atom environment of each Ba^{2+} ion is anisotropic in $Y_1Ba_2Cu_3O_{7-\delta}$ for all values of $\delta = 0.0-1.0$, because the Cu(1) atom plane contains fewer O^{2-} ions than does the Cu(2) atom plane. In $Y_1Ba_2Cu_3O_{7-\delta}$ the extent of the anisotropy of the oxygen atom environment is enhanced with increasing δ, because it is the oxygen atoms O(1) that are primarily lost [47,48,52]. With increasing oxygen concentration, the Coulomb attraction of the Ba^{2+} ion and the Coulomb repulsion of O(4) atom toward the O^{2-} ions of the Cu(1) atom plane become stronger, so that the capping oxygen atom O(4) moves father away from, while the Ba atoms and hence the CuO_2 layers move closer to, the Cu(1) atom plane. Consequently, as the oxygen concentration of the Cu(1) atom plane increases, the Cu(1)-O(4) distance increases, while the Cu(2)-O(4) distance decreases [53]. Namely, the Cu(2)-O(4)-Cu(1)-O(4)-Cu(2) linkages become shorter with increasing oxygen concentration, which will strengthen the interlayer interaction in each $Ba_2Cu_3O_{7-\delta}$ slab that occurs via the Cu(0)-O(4)-Cu(1)-O(4)-Cu(2) linkages.

3.5.3. **Comparison With the Experimental Results**

A. For the Normal High Pressure Sample

According to Cava et al.[49], the spatial arrangement of the oxygen atoms, and not only their average concentration, determines the superconducting transition temperature.

In our high pressure experiment, since the capsule loading with the sample is sealed, there is no chance for oxygen loss and other metallic elements (Y, Ba, Cu) loss. Also, under the 100 Kbar (10 GPa) and 925°C environment we can estimate the oxygen pressure inside the capsule is very high (estimated to be about 0.5 to 1 GPa). It would be reasonable to expect that under the high oxygen pressure and high temperature in the capsule, more oxygen atoms rearrange themselves into the proper position, thus we increase the oxygen concentration on the Cu(1) atom plane, so we strengthen the interlayer interaction in each $Ba_2Cu_3O_{7-\delta}^{16}$ slab that consequently, we increase T_C.

But I think the most direct evidence should come from the high resolutions electron microscope (HREM) images, and determination of δ of high pressure samples (e.g. using the comparative thermogravimetric analysis) although we have not done because of the experimental conditions restricted.

B. For the Isotopic Sample

From their neutron diffraction studies, the Argone group [82] found that oxygen upon heating evolves from different lattice sites with different degrees of freedom; especially the O(4) site being the most difficult to substitute. It would be reasonable to expect that under the 100 Kbar (i.e. high ^{18}O pressure inside the capsule), and 925°C in the capsule, more ^{18}O atoms substitute ^{16}O atoms especially O(4) site. This might be the reason why we observe the decrease in T_C for ^{18}O high pressure sample. As for the fact that T_C of pressurized $Y_1Ba_2Cu_3O_{7-\delta}^{18}$ sample is non-reversible by resubstitution of ^{16}O for ^{18}O at 500°C but reversible by resubstitution of ^{16}O for ^{18}O at 900°C under normal pressure, I can explain in the following way. If we check the phase diagram Fig 3.28 [56], we find that at 500°C, the material is in orthorhombic phase that the oxygen atoms ordering onto the (0, 1/2, 0) site which results in one-dimensional, "fencelike" CuO_3 chains parallel to the b axis as shown in Fig 3.26(a). While at 900°C, the material is in tetragonal phase showing a disordering of oxygen atoms in the same plane which results in the destruction of the novel one-dimensional CuO_3 chains as shown in Fig 3.26(b). I believe that it might be easier to substitute ^{16}O for ^{18}O atoms while the oxygen atoms in disordering state, and at 900°C the oxygen atoms have higher kinetic energy than that at 500°C; which means it has larger possibility that 16O atoms substitute ^{18}O atoms on O(4) site. This might explain why we observed T_c back up when oxygen exchanged at 900°C rather than at 500°C.

3.6. **The Relationship Between These Two Models**

The 1-2-3 structure of the $Y_1Ba_2Cu_3O_x$ system, $6 \le x \le 7$, has a unique property - the so called "oxygen sponge", i.e. when cooling from the sintering temperature, T_s ,usually around 950°C, oxygen content increases monotonically (Fig 3.28)[56] and when heating up, oxygen content decreases. The oxygen disorder-order induced phase transition from the semiconducting tetragonal structure to the superconducting orthorhombic structure is accompanied by the formation of coherent twins at temperature T_p, usually around 700°C, and

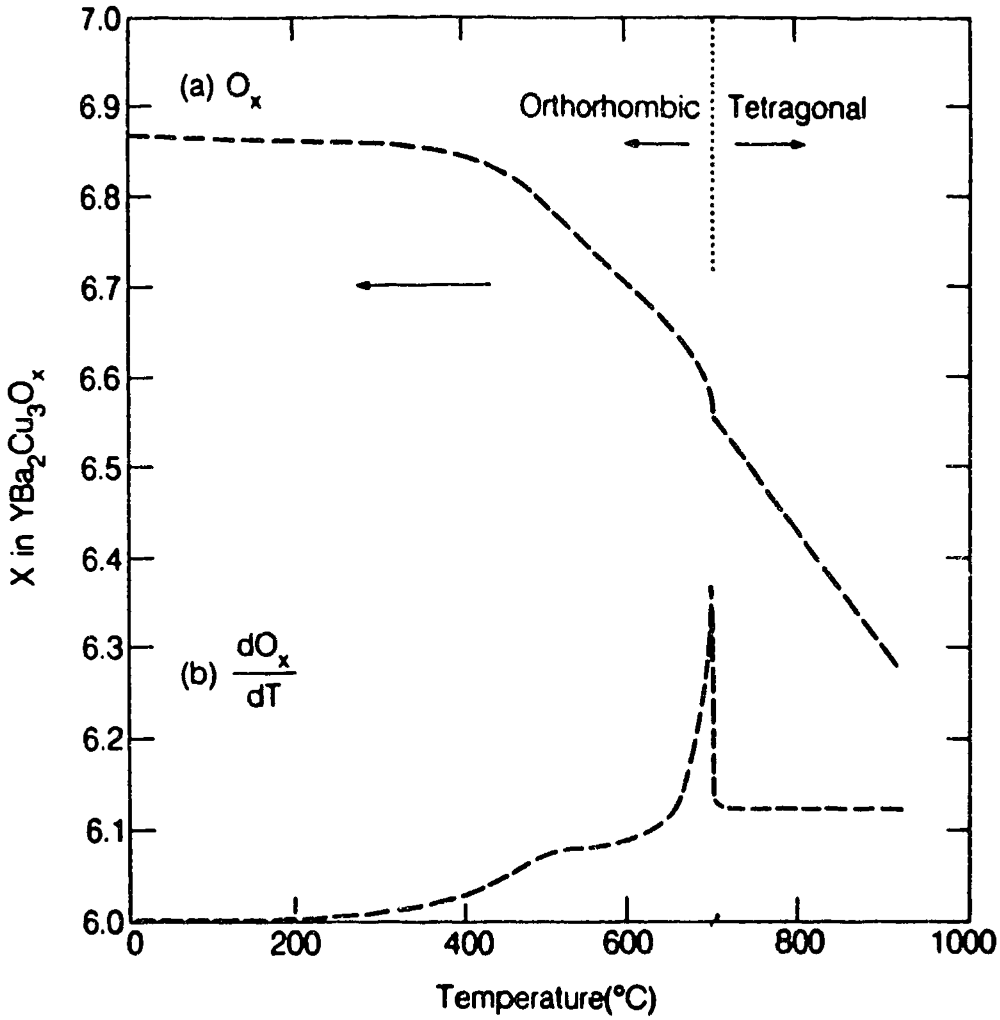

Fig 3.28. (a) Total oxygen content, x, in $Y_1Ba_2Cu_3O_x$ increases monotonically when cooled slowly from sintering temperature in 1 atm. O_2 ambient. (b) The differentiation of the curve in (a). (after Jou et al.[56]).

oxygen concentration $(O_x)_p$. Below T_p, the structure is orthorhombic with oxygen content $O_x > (O_x)_p$ when cooled slowly in an oxygen-rich ambient from the sintering temperature T_s. Above T_p, the structure is tetragonal with $O_x < (O_x)_p$. The rate of oxygen uptake increases sharply at T_p as shown in Fig 3.28(b). It is suggested [56] that the sudden increase of oxygen absorption rate is associated with a nucleation process, the formation of embryos of the orthorhombic phase. The twin boundaries are formed during the growth of the b-chain embryos which are first nucleated heterogeneously at grain surfaces. The oxygen-depleted twin boundary zones which serve as the primary oxygen diffusion paths from grain surfaces toward the interior of the grains, control the growth rate of the twins in the grain centers. The width of oxygen-depleted twin boundary zones should be determined by the balance of the chemical potential energy at the ends of b-chains at the edges of twin domains and the Coulomb repulsion energy between oxygen ions on the opposite sides of the twin boundaries. The rapid rate increase of oxygen uptake at T_p is attributed to a high oxygen vacany concentration in the grain during early stages of tetragonal to orthorhombic transformation caused by the formation of embryos which quickly consume a large fraction of the oxygen in the grain at T_p. Completion of the transformation by growth of twins occurs most rapidly at the grain surfaces by absorbing oxygen from the ambient and more slowly in grain interiors. Coarsening of the twin domains then occurs by elimination of small domains included within larger domains by localized transfer of oxygen atoms across the twin boundaries. This coarsening process takes place during annealing, resulting in residual stress relaxation and reduction of oxygen vacanies within the twin domains. Twin boundaries are essentially regions of tetragonal phase, about one unit cell thick, that have not been transformed into the orthohombic phase.

Oxygen-depleted twin boundaries with stoichiometric $Y_1Ba_2Cu_3O_{<6.5}$ have CuO_2 planes but are missing the Cu-O chains. Cu at the twin boundaries is in the fundamental oxidation state, Cu^I. Thus the resonance of the Cu frame would not propagate across the twin boundaries, i.e., these twin boundaries are in a nonsuperconducting state. Analysis of high T_c superconductors [57,58] indicate that they have extremely short coherence lengths, of the order of the size of the unit cell. e.g. the zero temperature coherence lengths $\xi(0)$ is a value of about 12 A in $Y_1Ba_2Cu_3O_7$. Because of the very small value of $\xi(0)$, insulating twin boundaries together with the twin domains on both sides form a superconductor-insulator-superconductor (SIS) Josephson junction. (A similar situation exists at the grain boundaries.) Inside a grain or crystal, the (1 1 0) and /or $(1\ \bar{1}\ 0)$ twin boundaries together with the (0 0 1) 90° -rotation boundaries or grain boundaries would form a three dimensional network dividing the grain into many superconducting clusters weakly coupled by SIS Josephson junctions i.e. a superconducting glassy state. The junctions should be particularly weak for (0 0 1) twins, in view of the extremely small value of $\xi(0)$ along the c axis. Such a superconducting glassy state includes intra- and inter-grain Josephson junctions. It would be expected that such a superconducting glassy state results in a significant reduction of average current density in polycrystalline oxide superconductors especially when the temperature is near T_C [59].

3.7. Further Discussion of the Isotope Sample

Since the discovery of superconductivity above 90K in $Y_1Ba_2Cu_3O_{7-\delta}$ [1,2], it has been debated whether the superconductivity in this material is phonon mediated as expected from the conventional BCS theory [60,65], or whether a different mechanism is involved. According to the conventional BCS treatment, T_C should vary as $M^{-\alpha}$, where M is the isotopic mass of atoms, and α is usually close to 0.5 for the full isotope effect. So

$$\alpha = -\frac{\delta T_c}{T_c}\frac{M}{\delta M} \qquad 3.18$$

If other mechanism without isotope effects are present, Eq.(5.1) will still be useful as an experimental measure for the electron-phonon interaction possibly present. Batlogg et al.[60], reported that the superconducting transition temperature, T_C does not change significantly when ^{16}O is replaced with ^{18}O in $Y_1Ba_2Cu_3O_{7-\delta}$. However the oxygen isotope effect was observed with a small decrease in T_C of 0.3 to 0.5K (α value of 0.03 to 0.05) in $Y_1Ba_2Cu_3O_{7-\delta}$ by Leary et al.[61] using susceptibility and by Katayama-Yoshida et al.[62] using resistivity measurement. Both Leary and Katayama-Yoshida groups considered their results important regarding the role of phonons in the electron-pairing mechanism. When we compare the sample preparing process of Batlogg et al., Leary et al., and Katayama-Yoshida et al., we find that Batlogg group exchanged ^{18}O for ^{16}O at 500°C while the other two groups exchanged ^{18}O for ^{16}O at about 900°C. But, owing to the smallness of α, other mechanisms for the occurrence of superconductivity, which are expected to be independent of isotopic mass, have been considered with vigor theoretically, ranging from plasmonic, excitonic, magnon-related effects to resonance valence bond (RVB) theory [63].

From above discussion, we can see the importance of isotope effect experiments in understanding the mechanism of high T_C superconducting materials. We use high pressure apparatus to press the isotope sample and substitute ^{16}O for ^{18}O at 500°C, and 900°C under the normal pressure. We observed the oxygen isotope effect, that is: after pressurized of both $Y_1Ba_2Cu_3O^{16}_{7-\delta}$ and $Y_1Ba_2Cu_3O^{18}_{7-\delta}$ samples, there is a small decrease in T_C of about 0.6 K at low magnetic field, and this shift of T_C is non-reversible by resubstitution of ^{16}O for ^{18}O at 500°C but reversible by resubstitution of ^{16}O for ^{18}O at 900°C under normal pressure. I think this consistents with the results of both Batlogg and Leary, Katayama-Yoshida groups.

Now, we estimate α at 10 Gauss. We take 2-IT-1 180 (HP) as the initial one, so T_{c_0} = 91.78K, T_{c_1} = 92.40K; M_0 = 18, M_1 = 16 $\delta T_c = T_{c_1} - T_{c_0}$ = 92.40 - 91.78 = 0.62K; δM = M_1 - M_0 = 16 - 18 = -2. So

$$\alpha = -\frac{\delta T_c}{T_{c_1}}\frac{M_1}{\delta M} = -\frac{0.62}{92.40}\frac{16}{(-2)} \doteq 0.05$$

This result is consistent with the results of Leary and Katayama-Yoshida groups.

In conclusion, the observation of the oxygen isotope effect of the high pressure samples suggests that the phonon mechanism is important for the electron-pairing in high T_c superconductivity of $Y_1Ba_2Cu_3O_{7-\delta}$. However owing to the smallness of α, the electron-phonon coupling alone is insufficient to explain such a high T_c in Y-Ba-Cu-O system, so that some additional enhancement mechanism may also be involved.

Chapter 4

Conclusions

This thesis has endeavored to present the work done on magnetic properties of high pressure $Y_1Ba_2Cu_3O_{7-\delta}$ superconductor over the past two years at Super-Press Lab and Physics Dept. of Univ. of Alberta. These two years represent a stepwise theoretical understanding and investigation of high pressure $Y_1Ba_2Cu_3C_{7-\delta}$ superconductor's magnetic properties.

X-ray measurements show that after pressurization, the lattice parameters a, b, and c do not change (in Table 3.4). This suggests that after pressurization the crystal structure of the sample has not changed. However, the X-ray data could not provide details of the oxygen atoms positions and occupancies.

SEM pictures show that after pressurization the grain size becomes smaller, about 1-5 μm (Fig 3.2 b,c) while the grain size is about 10 μm (Fig 3.2a) under the normal pressure. TEM picture (Fig 3.3) show that there are not fully grown twins between the the two fully grown twins boundaries, and there are microcracking on twin boundaries in some regions. All these properties are different from those of normal pressure samples. These might contribute to the unusual properties of high pressure samples such as higher T_C, lower upper field for the "quasi-de Almeida-Thouless" line, ect.

SQUID measurements show that the T_C of high pressure samples is about 1-1.4 K higher than that of the normal pressure one (Fig 3.16), and we got a "quasi-de Almeida-Thouless" line $H \propto [\ 1 - T/92.5\ ]^{3/2}$ up to 2000 Gauss for high pressure sample which is quite different from the results mentioned in [38]. According to our experimental results, we estimate the loop size in the order of 1000 A, which is about the order of twin spacings. We also found a magnetic phase diagram Fig 3.25 similar to the phase diagram proposed by Morgenstern et al.[32].

In superconducting-glass model: the quasi-AT line as found in the experiment can be explained as the phase boundary between the superconducting-glass phase and normal-conducting regime.

In oxygen concentration model: at the high pressure and high temperature environment, we may increase the oxygen concentration on the Cu(1) atom plane, thus we strengthen the interlayer interaction in each $Ba_2Cu_3O_{7-\delta}$ slab that occurs via the Cu(2)-O(4)-Cu(1)-O(4)-Cu(2) linkages, consequently we increase T_C.

As we know $Y_1Ba_2Cu_3O_x$, if x > 6.5, is in the superconducting phase which has an orthorhombic structure and is heavily twined; if x < 6.5, $Y_1Ba_2Cu_3O_x$ is in the nonsuperconducting phase which has a tetragonal structure, and is absent of TP's. The high density of twin boundaries is thought to occur as a result of the tetragonal-to-orthorhombic transformation. During this transformation, a given tetragonal grain does not usually seem to transform into a single orthorhombic domain. Rather the orthorhombic phase may nucleate into different parts of the grain, with the two possible $(\vec{a}, \vec{b})$ orientations, resulting eventually in the observed twin network. Because of the very small value of $\xi(0)$, these twin boundaries together with the 90°-rotation boundaries and grain boundaries divide the material into many superconducting clusters weakly coupled SIS Josephson junctions, i.e. superconducting glassy state.

A small decrease in T_C of about 0.6 K is observed when ^{16}O is substituted by ^{18}O for high pressure sample, and the shift is nonreversible by resubstitution of ^{16}O for ^{18}O at 500°C but is reversible by resubstitution of ^{16}O for ^{18}O at 900°C. The observation of the oxygen isotope effect of the high pressure samples suggests that the phonon mechanism is important for the electron-pairing in high T_C superconductivity of $Y_1Ba_2Cu_3O_{7-\delta}$. However, owing to the smallness of $\alpha(\alpha = 0.05)$, the electron-phonon coupling alone is insufficient to explain such a high T_C in Y-Ba-Cu-O system, so that other mechanisms for the occurrence of superconducivity may also be involved.

I should point out there are a lot of questions about high pressure experiment results to be answered, and there is a great deal of work still to be done, e.g. precisely determining δ, the critical current measurement, and heat capacity measurement, ect.

Whatever it is, interest in high temperature superconductivity is sure to remain high, both in the search for new materials and in the search for the underlying mechanism. The high pressure technique applied for high T_c superconductors here does provide incentive for further development work.

References

[1]. M.K. Wu, JR. Ashburn, C.J. Torng, P.H. Hor, R.L. Meng, L. Gao, Z.J. Huang, Y.Q. Wang, C.W. Chu, Phys. Rev. Lett. 58, 908 (1987).

[2]. P.H. Hor, L. Gao, R.L. Meng, Z.J. Huang, Y.Q. Wang, K. Froster, J. Vassilious, C.W. Chu, Phys. Rev. Lett. 58, 911 (1987).

[3]. J.G. Bednorz, K.A. Muller, Z. Phys. B. 64, 189 (1986).

[4]. C.W. Chu, P.H. Hor, R.L. Meng, L. Gao, Z.J. Huang, Y.Q. Wang, Phys. Rev. Lett. 58, 405 (1987).

[5]. J.E. Schirber, D.S. Ginley, E.L. Venturini, B. Morosin, Phys. Rev. B. 35 (16), 8709 (1987).

[6]. Y. Yamada, M. Yata, Y. Kaieda, H. Irie, T. Matasumoto, Jpn. J. Appl. Phys. Lett. 28 (5), L797 (1989).

[7]. P. Meuffels, R. Naeven, H. wenzl, Physica C 161, 539 (1989).

[8]. C. Allgeier, J. Heise, W. Reith, J.S. Schilling, K. Andress, Physica C 157, 293 (1987).

[9]. N. Kawahara, H. Enami, Y. Kitoh, T. Shinohara, S. Kawabata, H. Hoshizaki, A. ?Matsumnro, T. Imura, Jpn. J. Appl. Phys. Lett. 28 (4), L615 (1989).

[10]. J.G. Bednorz, M. Takashige, K.A. Muller, Eurpophys. Lett. 3, 379 (1987).

[11]. E. Ito, E. Takahashi, pp221 (1987) in "High-Pressure Research in Mineral Physics" (eds) M.H. Manghnani, Y. Syono, Terrapub, Tokyo 1987.

[12].T. Gasparik, "contributions to Mineralogy and Petrology, May 1988.

[13]. K. Wei, R.G. Trønnes, C.M. Scarfe (1990) JGR 95 (B10), 15,817 (1990).

[14]. T. Yagi, M. Akaogi, M. Arashi, T. Okai, K. Kawamura, K. Shino, M. Shimomura, K. Tabata, T. Suzuki, S. Akimoto, J. Geophys Res. 92, 6207 (1987).

[15]. K. Suito, "High Pressure Research Application to Geophysics", M.H. Manghnani & S. Akimoto (eds), San Diego, Calif. 1977 pp255.

[16]. I.C. Getting, G.C. Kennedy, J. Appl. Phys. 41, 4552 (1970).

[17]. C.T. Hertzberg, H. Sawamoto, Submitted to J. Geophys. Res. 1990.

[18]. B.D. Josephson, Phys. Lett. 1, 251 (1962); Adv. Phys. 14, 419 (1965).

[19]. J.E. Zimmerman, P. Thiene, J.T. Harding, J. Appl. Phys. 41, 1572 (1970).

[20]. J.E. Mercerean, Rev. Phys. Appl. 5, 13 (1970); M. Nisenoff, Rev. Phys. Appl. 5, 21 (1970).

[21]. R.P. Giffard, R.A. Webb, J.C. Weatley, J. Low Temp. Phys. 6, 533 (1972).

[22]. R.J. Cava, B. Batlogg, R.B. van Dover, D.W. Murphy, S. Sunshine, T. Siegrist, J.P. Remeika, E.A. Rietman, S. Zahurak, G.P. Espinosa, Phys. Rev. Lett. 58, 1676 (1987).

[23]. R. Beyers, G. Lim, E.M. Engler, R.J. Savoy, T.M. Shaw, T.R. Dinger, W.J. Gallagher, R.L. Sandstorm, Appl. Phys.

Lett. 50 (26), 1918 (1987).

[24]. G.W. Pei, J. Yan, Y.T. Liu, D.Y. Song, M.G. Lin, B.R. Lin, S.Y. Lin, X.M. Yang, G.S. Wang, Prog.in High Temp. Supercond. Vol 2, 165 (1987).

[25]. K.A. Muller, M.Takashige, J.G. Bednorz, Phys. Rev. Lett. 58 (11), 1143 (1987).

[26]. C. Ebner, D.Stround, Phys. Rev. B 31 (1), 165 (1985).

[27]. S.F. Edwards, P.W. Anderson, J.Phys. F.: Metal Phys. 5, 965 (1975).

[28]. S. Teitel, C. Jayaprakash, Phys. Rev. B 27, 598 (1983).

[29]. S. Teitel, C. Jayaprakash, Phys. Rev. Lett. 51, 1999 (1983).

[30]. W.Y. Shih, D. Stround, Phys. Rev. B 28, 6575 (1983).

[31]. C. M. Soukoulis, G.S. Grest, K. Levin, Phys. Rev. Lett. 50, 80 (1983).

[32]. I. Morgenstern, K.A. Muller, J.G. Bednorz, Z. Phys. B 69, 33 (1987).

[33]. S. John, T.C. Lubensky, Phys. Rev. Lett. 55, 1014 (1985).

[34]. G. Toulouse, Commun. Phys. 2, 1151 (1977).

[35]. J.R.L. de Aleida, D.J. Thouless, J. Phys. A. 11 (5), 983 (1978).

[36]. D. Sherrington, S. Kirkpatrick, Phys. Rev. Lett. 35, 1792 (1975).

[37]. T.R. Dinger, T.K. Worthington, W.J. Gallher, R.L. Sandstrom, Phys. Rev. Lett. 58, 2687 (1987).

[38]. A.P. Mulozemoff in Prog.in Hiigh Temp. Supercond. Vol. 6, " The Physical Properties of High T_C Superconductors, D.M. Ginsberg eds (1988).

[39]. M.A. Beno, L. Soderholm, D.W. Capone II, D.G. Hinks, J.D. Jorgensen, I.K. Schuller, C.U. Segre, K.Zhang, J.D. Grace, Appl. Phys. Lett. 51, 57 (1987).

[40]. J.E. Greedam, A. O'Reilly, C.V. Stager, Phys. Rev. B 37, 8770 (1987).

[41]. J.J. Capponi, C. Chaillout, A.W. Hewat, P. Lejay, M. Marezio, N. Nguyen, B. Raveau, J.L. Sonbeyroux, J.L. Tholence, R. Tournier, Europhys. Lett. 3, 1301 (1987).

[42]. W.I.F. David, W.T.A. Harrison, J.M.F. Gunn, M.A. Beno, D.W. Capone II, D.G. Hinks, I.K. Schuller, L. Soderholm, C.U. Segre, K. Zhang, J.D. Grace, Nature 327, 310 (1987).

[43]. Z. Fisk, J.D. Thompson, E. Zirngiebl, J.L. Smith, S.W. Cheong, Solid State Comm. 62, 743 (1987).

[44]. L.C. Porter, R.L. Thorn, U. Geiser, A. Umezawa, H.H. Wang, W.K. Kwok, H.C. Kao, M.R. Monagham, G.W. Grabtree, K.D. Carlson, J.M. Williams, Inorg. Chem. 26, 1645 (1987).

[45]. M.-H. Mhangbo, M.Evain, M.A. Beno, J.M. Williams, Inorg. Chem. 26, 1831 (1987)

[46]. M.-H. Whangbo, M. Evain, M.A. Beno, J.M. Willams, Inorg. Chem. 26, 1832 (1987).

[47]. A. Renault, G.J. McIntyre, G. Collin, J.P. Pouget, R. Comes, J. Physique 48, 1407 (1987).

[48]. M. Onoda, S.I. Shamoto, M. Sato, S. Hosoya, Jpn. J. Appl. Phys. 26, L876 (1987).

[49]. R.J. Cava, B. Batlogg, C.H. Chen, E.A. Rietman, S.M. Zahurak, D. Werder, Phys. Rev. B. 36 (10), 5719 (1987).

[50]. B.W. Veal, J.D. Jorgensen, G.W. Crabtree, W. Kwok, A. Umezawa, A.P. Paulikas, L.R. Morss, E.H. Appelman, L.J. Nowicki, L. Nunez, H. Claus, Intern. Conf. on Electron. Struct. and Phase Stability in Adv. Ceramics, Aug 17-19, 1987. Argonne National Lab, Argonne, Illinois, U.S.A.

[51]. D.C. Johnston, A.J. Jacobson, J.M. Newsam, J.T. Lewandowski, D.P. Goshoru, D. Xie, W.B. Yelon, Symposium on Inorganic Supercond. Amer.Chem. Soc. National Meeting, Aug.31-Sept.4, 1987, New Orleans, Louisiana, USA.

[52]. M.-H. Whangbo, M. Evain, M.A. Beno, J.M. Williams, Inorg. Chem. 26, 2566 (1987).

[53]. M.-H. Whangbo, M.Evain, M.A. Beno, J.M. Williams, "High Temperature Superconducting Materials" (eds. W.E. Hatfield, J.H. Miller, Jr.) 1988.

[54]. B. Batlogg, R.J. Cava, A. Jayaraman, S. Sunshine, D.W. Murphy, L.W. Rupp, H.S. Chen, A. White, K.T. Short, A.M. Mujsce, E.A. Rietman, Phys. Rev. Lett. 58 (22), 2333 (1987).

[55]. L.E. Murr, C.S. Nion, S. Jin, T.H. Tiefel, A.C.W.P. James, R.C. Sherwood, T. Siegrist, Appl. Phys. Lett. 55 (15), 1575 (1989).

[56]. C.J. Jou, J.Washburn "Studies of High Temp. Supercond." (eds. Anant Narlikar) Vol.1, PP229, 1989.

[57].see the review of J. Bardeen, in "Proceedings Mechanisms of Supercond., Berkeley, Calif.,1987", eds. S.A. Wolf & V.Z. Kresin (Plenum, NY, 1987)

[58]. T.K. Worthington, W.J. Gallagher, T.R. Dinger, Phys. Rev. Lett. 59, 1160 (1987).

[59]. G. Deutscher, K.A. Muller, Phys. Rev. Lett. 59, 1745 (1987).

[60]. J. Bardeen, L.N. Cooper, J.R. Schrieffer, Phys. Rev. 106, 162 (1957).

[61]. K.J. Leary, H.-C. Zur Loye, S.W. Keller, T.A. Faltens, W.K. Ham, J.N. Michads, A.M. Stacy, Phys. Rev. Lett 59, 1236 (1987).

[62]. H. Katayama-Yoshida, T. Hirooka, A.J. Mascarenkas, Y. Okabe, T. Takahashi, T. Sasaki, A. Ochiai, T. Suzuki, J.I. Pankove, T. Ciszek, S.K. Deb, Jpn. J. Appl. Phvs. 26, L2085 (1987).

[63]. "Novel Supercond." eds. S.A. Wolf, V.Z. Kresin,(Plenum, NY, 1987).

Proceedings of the International Conf. on High Temp. Supercond. & Materials and Mechanisms of Supercond., Interlaken, Switzerland, 1988. J. Muller, J.L. Olsen, (eds). Physica C 153-155 (1988).

[64]. M. Grimsditch, D.G. Hinks, J.D. Jorgensen, M.A. Beno, J.Z. Lin, H.B. Schuttler, C.U. Segre, L. Soderholm, B.W. Veal, I.K. Schuller, Phys. Rev. Lett 60, 752 (1988). A. Zettl, J. Kinney, ibid 753. B. Batlogg, R.J. Cava, M. Stavola, ibid, 754.

[65]. J. Bardeen, L.N. Cooper, J.R. Schrieffer, Phys. Rev. 108, 1175 (1957).

[66]. J.P. Franck, J. Jung, G. Salomons, W.A. Miner,

M.A.-KI. Mohamed. J. Chrzanowski, S. Gygax, J.C. Iriwin, D.F. Mitchell, G.I. Sproule. to be published in Physica C (1990).

[67]. J.D. Jorgensen, M.A. Beno, D.G. Hinks, L. Soderholm, K.J. Volin, R.L. Hitterman, J.D. Grace, and I.K. Schuller, C.U. segre, K. Zhang, M.S. Kleefisch, Phys. Rev B 36 (7), 3608 (1987).